

Topical Review

Controlling magnetism on metal surfaces with non-magnetic means: electric fields and surface charging

Oleg O Brovko, Pedro Ruiz-Díaz, Tamene R Dasa and Valeri S Stepanyuk

Max-Planck Institut für Mikrostrukturphysik, Halle, Germany

E-mail: obrovko@mpi-halle.de

Received 6 September 2013, revised 22 October 2013

Published 12 February 2014

Abstract

We review the state of the art of surface magnetic property control with non-magnetic means, concentrating on metallic surfaces and techniques such as charge-doping or external electric field (EEF) application.

Magneto-electric coupling via EEF-based charge manipulation is discussed as a way to tailor single adatom spins, exchange interaction between adsorbates or anisotropies of layered systems. The mechanisms of paramagnetic and spin-dependent electric field screening and the effect thereof on surface magnetism are discussed in the framework of theoretical and experimental studies.

The possibility to enhance the effect of EEF by immersing the target system into an electrolyte or ionic liquid is discussed by the example of substitutional impurities and metallic alloy multilayers.

A similar physics is pointed out for the case of charge traps, metallic systems decoupled from a bulk electron bath. In that case the charging provides the charge carrier density changes necessary to affect the magnetic moments and anisotropies in the system.

Finally, the option of using quasi-free electrons rather than localized atomic spins for surface magnetism control is discussed with the example of Shockley-type metallic surface states confined to magnetic nanoislands.

Keywords: magnetism, control, electric field, charging

(Some figures may appear in colour only in the online journal)

Contents

1. Introduction: conventional and novel ways of controlling magnetism	2	2.1. Effect of electric field at metal surfaces	5
1.1. Conventional (magnetic) ways of controlling magnetism at the nanoscale	2	2.2. Effect of electric field on the magnetic properties of single sub-nanoscale units	5
1.2. Controlling magnetism with non-magnetic means	2	2.3. Effect of electric field on magnetic anisotropy energy in nanochains	7
1.3. Electric field and charge at metallic surfaces: mechanisms	3	2.4. Tuning magnetic properties of thin films with external electric field and quantum well states	8
2. Controlling magnetism with electric fields	4	3. Surface charging with electrolytes	10
		3.1. Layered metallic systems	10
		3.2. Single impurities	12
		3.3. Impurity pair interaction	13

4. Direct surface charging: control of MAE and exchange interaction	15
4.1. Fe–Pt multilayers	16
4.2. Spin and orbital moments of Fe–Pt multilayers	16
4.3. Electronic structure analysis: decomposed density of states	17
4.4. Relationship between MAE and orbital anisotropy	18
5. Surface electron polarization controlled by electron confinement and electric field	18
5.1. Surface states and local magnetic properties	18
5.2. Spin-polarized surface states on Co nanoislands	19
5.3. Standing wave patterns and TMR	21
6. Conclusions	22
Acknowledgments	22
References	22

1. Introduction: conventional and novel ways of controlling magnetism

In recent decades striving for progress in magnetic data storage has become the standard motivation and the traditional theme for the introductory paragraphs for most papers dealing with magnetic phenomena, be they of fundamental or engineering character, experimental or theoretical. Today, after years of productive research and development, the future of data storage and processing is still considered to lie in the utilization of the spin degree of freedom, so called spintronics [1, 2] or magneto-electronics [3]. Quite recently a new trend has emerged—magnonics [4], a new branch of solid state research, competing with spintronics for the right to achieve a breakthrough in energy efficient and fast data storage and processing. The study of the behavior of spin waves in nanostructures and magnetization reordering due to spin precession has already yielded a few promising examples of spin-wave or magnetic logic [5, 6].

The actual technological applications have also been closely following the milestone discoveries of fundamental effects. For example, the giant and tunneling magnetoresistances have quickly made their way into the read heads of modern hard disk drives [7]. The most noteworthy fact, however, is that the write heads, in contrast to their read counterparts, are still using magnetic coils and fields to store information in the magnetization state of ferromagnetic bit domains and have been doing so since the earliest storage devices, such as magnetic tapes [7], although the accessible size of one bit has shrunk by several orders of magnitude over time, and novel methods, e.g. heat-assisted magnetic recording (HAMR) [8], are continuously being developed and implemented. Nevertheless, this goes to show that sensing magnetism on the nanoscale is much easier than controlling it.

In the present review, after briefly outlining the overall scope of possibilities to control magnetism, we focus on a particular class of systems that has recently moved into the field of attention of the community—metallic surfaces—and review the possibilities to locally tailor their magnetic properties with external electric fields (EEFs) and surface charging.

1.1. Conventional (magnetic) ways of controlling magnetism at the nanoscale

As already mentioned above, when it comes to controlling magnetization there is barely a more universal tool, than magnetic field. It has, however, a major drawback. While the whole research and development in the field of magnetism is on the miniaturization trip, magnetic field with its inherent non-locality is a major hindrance on that road. A possible work-around is the use of electron spin both as a carrier of information and as a switching tool. This concept is the basis for modern spin-transfer torque [9, 10] based devices [11, 12].

1.2. Controlling magnetism with non-magnetic means

It seems, however, much more promising to use alternative mechanisms to control the magnetization and atomic spins on the nano- and meso-scales. Active research of recent years has yielded quite a few such possibilities. One of the most studied fundamental effects nowadays is the effect of magneto-electric coupling [13, 14], found, for example, in multiferroic materials [15–22]. Though pioneering works in this area can be dated to the 1950s and 1960s, there has been a recent revival and surge of interest in the subject driven by technological hopes and aspirations.

1.2.1. Multiferroics. Multiferroics owe their popularity to the innate effect of magneto-electric coupling, which defines them as a class of materials. As the name hints, the main property making multiferroic materials interesting is the coexistence therein of two ferric properties—ferroelectricity and ferromagnetism, coupled to each other. This coupling makes it possible to control magnetic properties of the material by applying electric bias and vice versa. Considerable effort has been invested in finding novel materials exhibiting multiferroicity. It was shown that magneto-electric coupling in multiferroics can be used to control magnetic and ferroelectric phases [23, 17], magnetic ordering and domains [24–27], as well as anisotropy, coercivity and magnetic hysteretic behavior [28, 29]. Among other uses, multiferroicity can be a useful tool for the emergent field of magnonics, as it allows a certain degree of control over the spin-wave frequency (e.g. in BiFeO₃) using electric fields as a regulating tool [30]. Other studies have shown that electric field can induce a change in the direction of anisotropy in the ferromagnet, coupled to a multiferroic [31].

1.2.2. Magnetic semiconductors. Another way to couple electric field and magnetic properties is by manipulating the concentration of charge carriers and consequently the magnetic order. This scheme has been implemented in magnetic semiconductors based on Mn-doped InAs [17]. The gate voltage controls the concentration of holes mediating the interaction between Mn dopants. Unfortunately, both the latter and the ferroelectric approaches have a major drawback: the critical temperature, at which thermal fluctuations destroy magnetic order, is too low for most semiconductors and multiferroics [32]. Only very recently a magnetic semiconductor, which allows us to switch its magnetic state from the paramagnetic to the ferromagnetic one at room temperature by means of the gate voltage, has been introduced [33].

1.2.3. Graphene. Another famous material exhibiting magneto-electric properties is graphene. A double layer of graphene was shown to sensitively react to EEF, exhibiting demagnetization due to charge redistribution and band-filling alteration [34]. Magnetization of Au and NO₂ adsorbates on graphene was shown to be continuously tunable with EF [35]. Graphene bilayers, exchange-bias coupled to a ferromagnetic oxide, are susceptible to spin-rotation control by EEF [36]. A graphite multilayer sandwiched between electrodes exhibits spin phase transition between FM and AFM states upon application of an external bias [37].

1.2.4. Molecules and nanodots. Electric field/bias is not an exclusive non-magnetic possibility to tailor magnetism. Vivid examples of this fact are magnetic-molecular materials and systems of nanodots. Typical examples of this type of material are solids based on spin-crossover [38–40] and bimetallic cyanide complexes [41–44]. In these materials light or pressure can often be used as physical stimuli to control the spin state. However, anisotropy in iron-based molecular magnets was shown to be sensitive to EEF as well [45]. Another nice example of easy electric control of the spin state of a molecular magnet are delocalized mixed-valence magnetic clusters [46].

Quantum dots of Mn_{0.05}Ge_{0.95} have been shown to change their ferromagnetic properties upon application of a gate-bias to a metal–oxide–semiconductor (MOS) capacitor containing the latter quantum dots in its channel [47]. Here the change in the hole concentration was found to be responsible for the change of magnetic properties.

1.2.5. Electric field in non-metals. As we have seen above, many non-magnetic ways of tailoring magnetism are based on the application of the electric field/bias. At the same time, the underlying mechanism can be totally different. For example, in non-metallic materials light and electric bias can generate an isothermal and reversible crossover between the para- and ferromagnetic phases, as has been shown on the example of a Cd_{0.96}Mn_{0.04}Te quantum well [48]. Electric field affects the electrons' spin dynamics via the spin–orbit interaction in magnetic semiconductors [49, 50]. Controlling isothermally and reversibly the transition temperature of ferromagnetism in a semiconducting alloy seems to be possible with electrolyte-assisted application of electric fields [51].

In composite structures magnetization can be tailored dynamically or statically by applying constant or changing EEF or bias. As an example such materials as Ni/Pb(Mg_{1/3}Nb_{2/3})O₃–PbTiO₃/Ni [52], metglas–Pb(Zr, Ti)O₃ [53], or CoFe₂O₄ films [54] can be mentioned. MgO with metallic ferromagnets (such as Fe or Fe-rich CoFeB) [55], Co_{0.6}Fe_{0.2}B_{0.2} [56], InAs quantum valves [57], Ba₂CuGe₂O₇ [58], (Ga, Mn)As/(Ga, Mn)(As, P) bilayers [59], EuTiO₃ [60], and CoFeB–MgO–CoFeB magnetic tunnel junctions [61] can also be mentioned as pronounced magneto-electric materials.

In the present review, however, we shall focus on a more transparent magneto-electric coupling mechanism, namely magnetism control on metallic surfaces with external electric fields and active surface charging. We shall show that this route leads to numerous possibilities to tailor the magnetization, magnetic anisotropies and magnetic interactions of the surface and the adsorbates thereon.

1.3. Electric field and charge at metallic surfaces: mechanisms

Let us first of all discuss the emergent physics that we expect to find when a metallic surface is exposed to EEF or additional charge. Of course the key role will be played by the conduction electrons freely available in a metal.

1.3.1. Electric field. When a surface of a metal is exposed to external electric field (figure 1(a)), the conduction electrons at the surface find themselves in a non-flat electrostatic potential (dashed line, upper panel) and strive to screen the field and even out the potential within the metal (solid line, upper panel) by redistributing their density (filled curves in the lower panel). In the case of a magnetic surface, electrons of different spin characters experience different degrees of redistribution, a phenomenon termed spin-dependent screening [62–64] (the solid and dashed curves in the lower panel of figure 1 are meant to illustrate screening charge with different electron spins).

Both spin-dependent and paramagnetic screening obviously change the concentration of charge carriers at the surface, changing the chemistry and thus affecting both structure and magnetism on the surface, the adsorbates thereon and magnetism-related processes in the system.

1.3.2. Charging with electrolytes. To create a perturbation in the electrostatic potential of the surface an EEF is not the only option. While the physics of electrolytes is complex and diverse and the models of solid–electrolyte interfaces can be of various complexities (see, e.g., [65]), the general picture (corresponding to one of the most widely used models, the Gouy–Chapman–Stern one) is the following [66, 65]. If a surface comes into contact with an electrolyte solution or ionic liquid (schematic diagram in figure 1(b)), the so called electric double (or multi-) layer is created at the interface. Due to the attraction of electrolyte's ions by the surface electronic charge, the ions accumulate at the surface, forming a charged layer (so called 'Stern' or 'Helmholtz layer'). The charge of that layer is partially screened by the surface electrons and partially by the opposite charge carriers in the electrolyte, forming the 'Gouy layer'. Since the Stern layer ions are adsorbed directly at the interface, the whole picture is somewhat analogous to the surface being exposed to an extremely strong electric field (see the plot in the upper panel of figure 1(b), analogous to the respective plot in figure 1(a)) [66]. In addition to intense charge redistribution, the electrolyte solution has a direct chemical influence on all processes at the surface. Both the chemical action and screening can strongly affect magnetism of adsorbates on or in the surface [66, 67]. However, inside the surface the effect of the electrolyte might be considered analogous to the application of a strong electric field, i.e. of purely electronic character. Finally, since the electrolyte surface layers can be controlled by an external bias [66], the use of electrolytes can be seen as an enhancement of the EEF application. Finally, before proceeding to other EEF and charging related phenomena, we want to stress that in this review we are not aiming at a complete and thorough description of all possible electrolyte-related phenomena, but are rather interested in electrolytes as means of controlling charge redistribution in metals in the spirit of Weisheit *et al* [66].

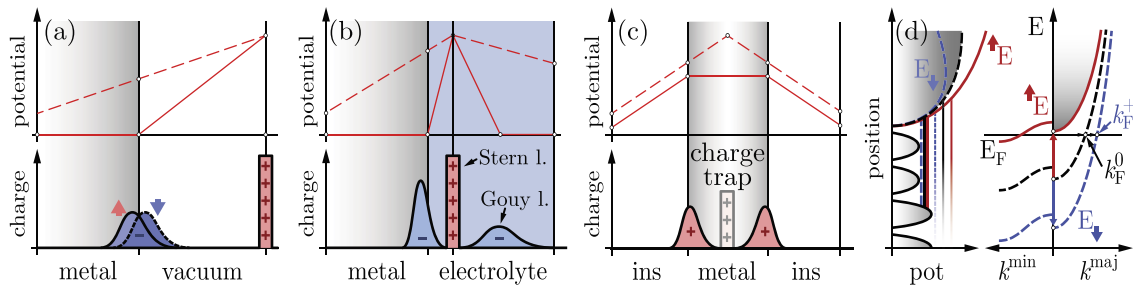


Figure 1. Mechanisms at work when a metallic surface is exposed to EEF or charging.

1.3.3. Direct charging of a metallic surface. Apart from the use of EEF and electrolytes, there is also a promising option of charging the surface directly. If the surface slab is electrically decoupled from the substrate, e.g. by an insulating spacer (figure 1(c)), the charge that is added to the surface slab will remain trapped in the latter, effectively doping it with electrons or holes. Considering the Coulomb repulsion, the charge is expected to diffuse towards the interfaces of the metallic slab, forming an electron or hole excess cushion (figure 1(c)), which will inevitably affect magnetic and electronic properties of the surface in a similar way as EEF or EDL does [68].

1.3.4. External electric field and surface state electrons. Finally, there exist somewhat exotic cases, such as the use of surface states, existing on certain noble-metal surfaces and behaving like a quasi-free 2D electron gas [69–72]. The dispersion relation in the plane of the surface has a parabolic character. However, on magnetic surfaces the surface state can be spin polarized [73], so that the free-electron behavior is observed only in one spin channel (figure 1(d)), or the effective parameters of the dispersion curve parabolas are different for electrons of different character. The energy position of the surface state bands was shown to exhibit a Stark-like shift under the influence of an external electric field (see sketch in figure 1(d)) [74]. This opens further intriguing possibilities to tailor electronic and magnetic properties at surfaces [75].

Let us now see how the fundamental mechanisms discussed above can be applied to the task of voluntarily tailoring the magnetism at surfaces.

2. Controlling magnetism with electric fields

One of the most interesting but also one of the trickiest tasks is the task of controlling the spin orientation of single magnetic adsorbates on a paramagnetic metallic surface. The necessity to do so is dictated by modern nanoscience and information technology striving to maintain continued technological progress. The interest in low-dimensional magnetic nanostructures (atomic-scale clusters, wires, molecular magnets) is justified by the hope of using atomic-size magnets as information storage units in spintronic applications [76–79].

One way of creating a switchable information bit lies in the use of atomic-scale units that exhibit magnetic bi- or multi-stability. This property is innate to magnets that have

two or more stable magnetic states with a relatively small energy gap between them (of the order of tens of meV). The existence of magnetic bistability was first reliably found in molecular magnets: $\text{Mn}_{12}\text{O}_{12}$ -acetate molecules [77–79]. First principles calculations gave a proper description of magnetic properties of these magnets in free space [80, 81] and on surfaces [82]. Of course, molecular magnets are not the only structures exhibiting magnetic bistability. Theoretical studies suggest that this phenomenon is much more common: it arises in nanostructures of different sizes and geometries, e.g. in supported Mn clusters on Ag [83] or in Mn and V clusters on Cu [84] surfaces.

The key question, of course, is how such bistable magnetic units can be switched between states. In principle it can be done by means of thermal activation [77, 85], magnetic field, pressure or light radiation [85]. These techniques, however, are inherently non-local, setting a severe limit to their applicability in high density data storage. A viable alternative is electric-field-controlled switching of magnetism.

Recent studies have shown that an EEF indeed dramatically affects physical properties of surface systems. It modifies not only adsorption energetics of individual atoms [86], but also the surface kinetics of adatoms [87, 88] and molecules [89]. EEF controls the structure, dimensionality and reactivity of supported metal nanoclusters [90]. Density functional studies have shown that an applied electric field can substantially improve the hydrogen storage properties of polarizable substrates, e.g. boron nitride sheets and slabs [91, 92].

Non-magnetic free-standing nanoparticles consisting of tens of atoms [93] exhibit ferromagnetism when exposed to an EEF. For non-metallic substrates it was theoretically predicted that the magneto-electric effect can arise at interfaces without the classically known volume multiferroicity [94]. *Ab initio* calculations have shown that spin-dependent EEF screening in Fe/BTiO₃ can change the magnetic moment of Fe and Ti atoms, thus changing the magnetization of the surface as a whole. In polar magnetic molecules, where the Stark effect competes with the super-exchange interaction for magnetism domination, EEF has been shown to play an important role in the struggle [95].

To understand how EEF can be used to control the magnetism of single adatoms we can first take a look at layered and mesoscopic systems.

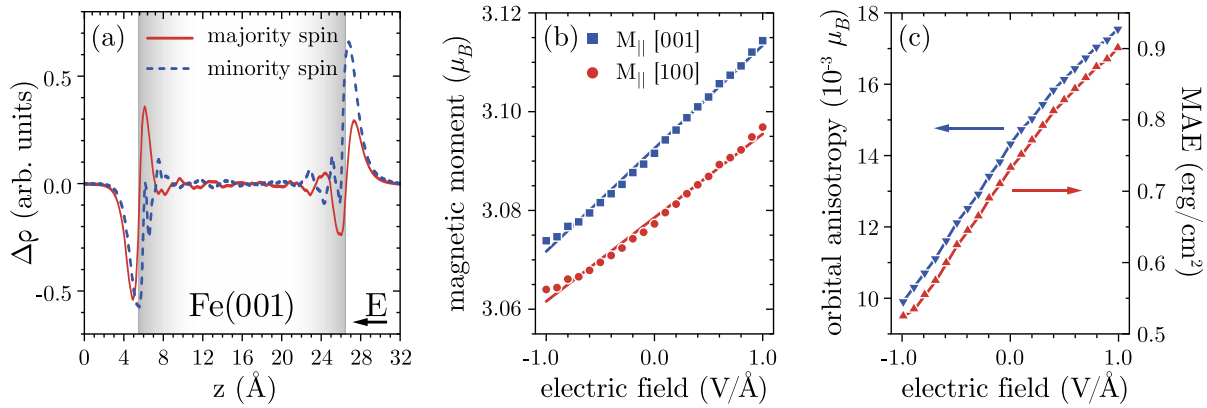


Figure 2. (a) Charge density redistribution induced by EEF in a 21 Å thick Fe film for majority- (solid line) and minority- (dashed line) spin electrons. The applied EEF is $\pm 1.0 \text{ V } \text{Å}^{-1}$, pointing from right to left. (b) Total magnetic moments on the (001) Fe surface as a function of applied electric field for the magnetic moment lying in the plane of the film (along the [100] direction) and perpendicular to the plane (along the [001] direction). The solid lines are a linear fit to the calculated data. (c) Electric-field-induced changes in calculated orbital moment anisotropy in units of $10^{-3} \mu_B$ of the surface Fe atom and surface magneto-crystalline anisotropy energy (MAE) for a 15 ML thick Fe(001) slab. Figures adapted from [99] (The American Physical Society copyright 2008).

2.1. Effect of electric field at metal surfaces

State of the art electron beam experiments [96], operating with pulses intense enough for the associated electric field to cause significant electron charge redistribution (screening), but short enough to make sure that atomic positions are not affected by electrostriction, have shown that a purely electronic response can cause a change in magnetic anisotropy and magnetization dynamics of a Co–Fe alloy film sample. These changes, however, are temporary and are observable on fairly short time scales.

Supported metal (Pd) thin films were shown to exhibit EEF-induced ferromagnetism [97]. Here, however, the mechanism is related to the material-specific Stoner instability [98]. The charge redistribution induced by the EEF changes the occupation of the Fermi level, thus toppling the delicate balance and inducing ferromagnetism, a change which is equally profound and hard to control precisely.

A more stable change in magnetic moment and anisotropy of the sample can be achieved by application of a constant EEF to ferromagnetic systems. The mechanism of spin-dependent screening, playing the main role in that case, has already been briefly introduced in section 1.3.1. Electrons of different spin characters show different responses to the external field, thus changing the local magnetization properties. Theoretical studies have shown that this scenario is realistic for metallic slabs. Duan *et al* [99] have predicted that ferromagnetic Fe, Ni and Co exhibit magneto-electric effects in the presence of EEF. The reason is indeed the spin-dependent screening of the EF. Figure 2(a) shows the calculated redistribution of majority- (solid line) and minority- (dashed) spin electrons in an Fe(001) slab under the influence of an external potential gradient. The spin dependence of the process is obvious. As a result, the electron or hole accumulations in different spin channels are different, thus changing not only the occupation at and around the Fermi level, but also the balance of majority and minority electrons directly. This leads to a change in the magnetic moments of interface atoms. Figure 2(b) shows the

dependence of the magnetic moment of the interface atoms of the slab featuring in figure 2(a) on the applied EEF. A near-linear trend can be clearly observed. Not only the magnetic moment shows a response to EEF, but also the orbital moment anisotropy [99, 100] and the magnetic anisotropy energy (see figure 2(c)). The fields considered in this work are quite realistic. However, the change in the magnetic moment and magnetic anisotropy are not quite enough to use that particular system in technological solutions. One possible way to enhance the effect of the EEF is to use electrolyte to additionally charge the surface by EEF [66, 101]. This possibility will be discussed in more detail in a later section.

In another paper [102] it was shown that using the EEF to manipulate the magnetic anisotropy dynamically could also allow one to facilitate or even force magnetization switching. A Landau–Lifshitz–Gilbert simulation showed the possibility of magnetization switching in a layered (Ga, Mn)As system between two different stable states through electric field control of magnetic anisotropy, with no external magnetic field, spin current, or mechanical stress involved. However, since here we concern ourselves with metal systems only, we shall not dwell on this topic.

2.2. Effect of electric field on the magnetic properties of single sub-nanoscale units

While we set out to find a tool for switching single magnetically bistable nanostructures at the surface, up to now we have been discussing 1D layered systems. Nevertheless, the general approach of using EEF to control magnetism at the surface can be applied to sub-nanoscale systems as well. To give a particular example, let us take a look at a trivial magnetic surface-supported system—a compact transitional metal dimer (Mn in this case) on a paramagnetic surface (here, Ag(001)) as is sketched in figure 3(a) [64]. The magnetism of the dimer is determined by the direct exchange interaction between the Mn atoms and is characterized by a collinear spin alignment

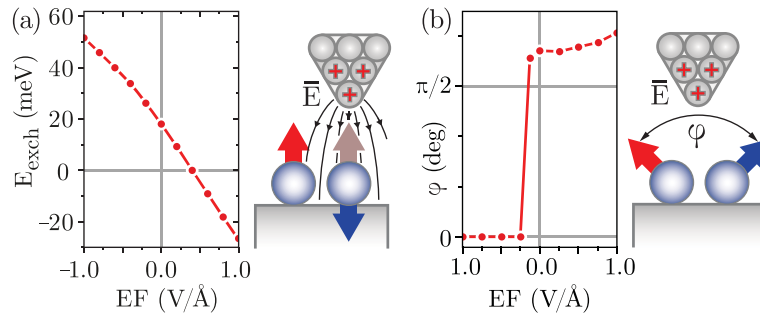


Figure 3. (a) Dependence of the exchange interaction in a compact Mn dimer on Ag(001) on the magnitude of the applied EEF. The sketch on the right depicts the principal setup of the computational experiment. (b) Angle between the spins of Mn atoms on a weakly magnetic Ni(001) surface as a function of the applied EEF. (Figures adapted with permission from [64] copyright (2011) The American Physical Society).

with two magnetic states: FM and AFM. Without external influences, the FM state is more stable, and the energy difference $E_{\text{exc}} = E_{\text{AFM}} - E_{\text{FM}}$ is calculated to be 18 meV, with Mn atoms having magnetic moments of $3.92 \mu_B$ [64]. If the dimer is exposed to external electric field, the E_{exc} values change dramatically (figure 3(a)). Fields with a field vector directed away from the surface (in the following ‘negative fields’) enhance the exchange to values as high as 50 meV at $EF = -1.0 \text{ V/\AA}$, while at positive EEF of $\sim 0.4 \text{ V/\AA}$ a reversal of the stability occurs. For $EF > 0.4 \text{ V/\AA}$ an AFM dimer is the ground state.

If the substrate is not paramagnetic, but has a magnetism of its own, an even more interesting situation can arise. Negulyaev *et al* [64] have predicted that a Mn dimer on Ni(001) has a very diverse energy landscape with respect to spin orientation of the two Mn atoms, making it a ‘multi-stable’ system with several closely lying metastable states. The weakly magnetic Ni(001) with a bulk magnetic moment of $0.65 \mu_B$ makes the ground state of the Mn dimer a non-collinear one (figure 3(b)) with an angle of 116° between the spins. Furthermore, the application of an EEF has a profound effect on that angle: a positive field slightly but smoothly increases it, while negative fields totally destroy non-collinearity, making the ferromagnetic alignment of spins the ground state of the dimer.

The origin of the magneto-electric effect in this case is complex [64]. On the one hand, the EEF affects positions of Mn atoms. Negative EEF lifts the dimers, since the positively charged Mn nuclei with the core electrons shift along the direction of an EEF. For $EF = -1.0 \text{ V/\AA}$, vertical separations of the FM and the AFM dimers from the surface are changed from $z_F = 1.64 \text{ \AA}$ and $z_A = 1.62 \text{ \AA}$ to $z_F = 1.75 \text{ \AA}$ and $z_A = 1.74 \text{ \AA}$ respectively. Positive field pushes the dimers into the substrate: for $EF = 1.0 \text{ V/\AA}$, $z_F = 1.63 \text{ \AA}$ and $z_A = 1.61 \text{ \AA}$. On the other hand, $EF > 0$ attracts electrons from the surface into the vacuum, thus increasing bonding between Mn atoms in FM and AFM dimers and decreasing their bond lengths (y_F and y_A), and vice versa. The values of y_F are found to be 2.72, 2.67, 2.65 \AA and y_A are 2.59, 2.49, 2.45 \AA for electric fields EF of $-1.0, 0$ and 1.0 V/\AA respectively [64].

To understand why EEF favors either ferro- or antiferromagnetic alignment of spins, the authors of [64] analyze

the electronic properties of the dimers. The FM and the AFM dimers have different spatial distributions of the valence electrons (4s, 4p, 3d). Figure 4(a) displays the cross section of the electron-density difference between the FM and the AFM dimers by a plane $x-z$ perpendicular to the surface and passing through the dimer (i.e. $n_{\text{FM}}(x, y = 0, z) - n_{\text{AFM}}(x, y = 0, z)$) in the absence of an EEF. The red (blue) color marks areas where the electron density of the FM dimer is larger (smaller) than that of the AFM one. Blue and red spots are situated differently with respect to the dashed horizontal line, which crosses the nuclei of the Mn dimers (figure 4(a)). This indicates that the electrons of the FM dimer are less localized near the surface and reach further into the vacuum than those of the AFM dimer. This difference can be understood from the electronic structure of the dimers. The spin-polarized local density of states (LDOS) of a Mn atom within the AFM dimer is shown with solid lines in figure 4(b): the majority electrons exhibit one single-atom-like peak at -2.4 eV and are localized in the central region of the dimer. The LDOS of a Mn atom within the FM dimer is shown with dashed lines in figure 4(b): the density of states of the majority electrons is split into two levels at -2.3 and -1.8 eV . This result correlates with the Alexander–Anderson model [103], which predicts a splitting of states in a FM dimer into bonding and anti-bonding orbitals. The bonding state is more tightly bound [103], which is reflected in the LDOS peak at -2.3 eV . The anti-bonding state is destabilized energetically (the peak at -1.8 eV) and localized in the outer region of the dimer [103]. These electrons penetrate deeper into the vacuum than those of the AFM dimer. The number of minority electrons of a Mn atom in the dimers is small, and the difference between their LDOSs (figure 4(b)) for $E < E_F$ is insignificant, thus they are out of the scope of further discussion [64].

Since the majority 3d electrons of the FM Mn dimer are destabilized energetically and penetrate into the vacuum more than those of the AFM dimer, they are more sensitive to external influences. As a proof [64], in figures 5(a) and (b) the LDOS of 3d electrons for the AFM and FM dimers at two extreme values of EF is shown. If EF switches from 1.0 to -1.0 V/\AA , the single peak in the LDOS of a Mn atom within the AFM dimer shifts by $\sim 70 \text{ meV}$ towards lower energies (figure 5(a)). This is the consequence of negative

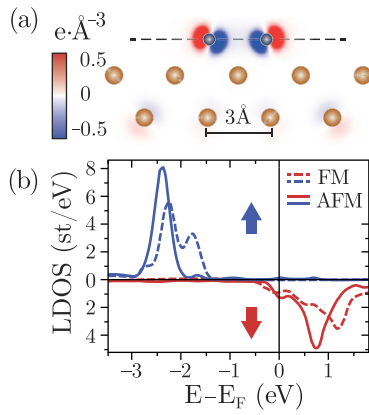


Figure 4. (a) Difference between the spatial distributions of electron density of the FM and the AFM Mn dimers on Ag(001) in the absence of an EEF. A crosscut by a plane $x = 0$ (see the coordinate system in figure 1(a)) is shown. Yellow balls—Ag atoms, blue balls—Mn atoms. The dashed line crosses the nuclei of the FM and the AFM dimers. (b) The spin-polarized LDOS of 3d electrons of a Mn atom within the FM dimer (dashed lines) and the AFM one (solid lines). (Adapted with permission from [64] copyright (2011) The American Physical Society).

EEF pushing the upper part of the electron clouds of the dimer towards the Mn nuclei, thus decreasing the potential energy of electrons. The peaks' shifts for the FM dimer are different: the low-energy peak shifts by ~ 70 meV, while the high-energy peak shifts by ~ 150 meV (figure 3(b)). The sensitivity to an EEF of the anti-bonding states in the FM case and their stronger shift towards higher energies at $E_F > 0$ leads to the higher total energy of the FM dimer, while the stronger shift towards the lower energies at $E_F < 0$ causes the lower total energy of the FM dimer. Despite the fact that the Ag(001) substrate was not involved in the discussion explicitly, its role is paramount. A free-standing Mn dimer is a weakly bonded van der Waals molecule with binding energy of the order of tens of millielectronvolts [104]. A Mn dimer on Ag(001) is a strongly bonded pair of atoms (binding energy 0.7 eV) with direct overlap of localized d orbitals. This is what makes controlling a magnetic ground state of the dimers by EEF possible in the first place.

To sum up the last few paragraphs, an electric field can be used for local control of magnetism and re-alignment of individual spins in low-dimensional magnetic nanostructures on magnetic and non-magnetic metal surfaces. The key role herein is played by the spin-dependent screening of the EEF by the surface and nanostructure electrons.

2.3. Effect of electric field on magnetic anisotropy energy in nanochains

As has been mentioned in section 1, dealing with thermal instability is a major challenge for many magneto-electric materials and applications. One of the things that can help to mitigate the magnetic instability is high magnetic anisotropy energy (MAE), which would stabilize magnetic moments against thermal fluctuations. There are a few materials that can provide the needed anisotropy values. Among the most

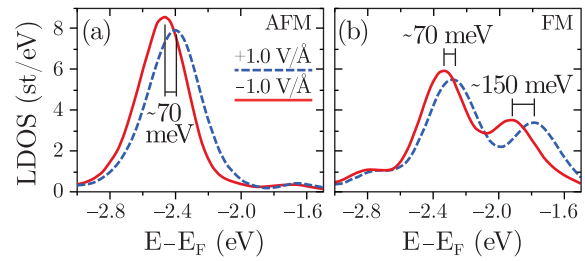


Figure 5. The LDOS of the majority 3d electrons of a Mn atom within (a) the AFM and (b) the FM dimer at two extreme values of field intensity (red curves, $E_F = -1.0$ V/Å; blue curves, $E_F = 1.0$ V/Å). (Adapted with permission from [64] copyright (2011) The American Physical Society).

promising ones are the 3d–5d transitional metal compounds, which have critical temperatures T_c far above room temperature [66]. The high T_c of these compounds is explained by the large magnetic anisotropy. Furthermore, they often have an out-of-plane easy axis of magnetization, which is often desirable in applications. Apart from the intrinsic properties of the materials, MAE is often enhanced in structures of reduced dimensions or reduced dimensionality. It was shown that 0D (adatoms) [105, 106] and 1D (chains and wires) [107–110] nanostructures on metal surfaces exhibit larger MAE than is encountered in the bulk of respective systems. An experimental study of Co/Pt(111) clusters showed that MAE per Co atom is inversely proportional to the cluster size. For a single Co adatom on Pt(111) a giant MAE of 9 meV was measured [105, 111, 112]. Large MAE of Co chains on the (997) surface of Pt was observed in another experimental study [108]. Nowadays, clusters and chains of various sizes and composition can be created on surfaces by self-assembly [113–115] or even by STM manipulation [116–121]. While the chemical composition and the size of the nanostructures are the defining parameters for its magnetic anisotropy, our interest lies in the possibility to flexibly affect the MAE by means of external electric fields. In fact, now we know that the latter affects the charge carriers at the metal/insulator(vacuum) interfaces [122, 13, 64, 74] and, what is even more important for technological applications, does so in a local way [122, 13]. Let us see what implications this might have for the magnetic properties of the system.

Magneto-electric coupling in complex alloys is often determined by the hybridization between the orbitals of the magnetic atoms and the non-magnetic ones having large spin-orbit coupling [123], or directly with the atoms of the surface [124]. Since charge carrier density directly affects hybridization, the application of EEF should have an indirect effect on the MAE of the system. Let us briefly illustrate this mechanism by the example of atomic chains and thin films [63].

In a recent paper by Dasa *et al* [63], it was shown, taking linear Co and Co–Pt chains on Pt(111) as a model system (figure 6(a)), that exposing such systems to EEFs not exceeding 1 V/Å can lead to a significant change of MAE of the system (by $\sim 34\%$, see figures 6(b) and (c)). The magnetic anisotropy energy was determined in an *ab initio* way, using fully relativistic self-consistent calculations

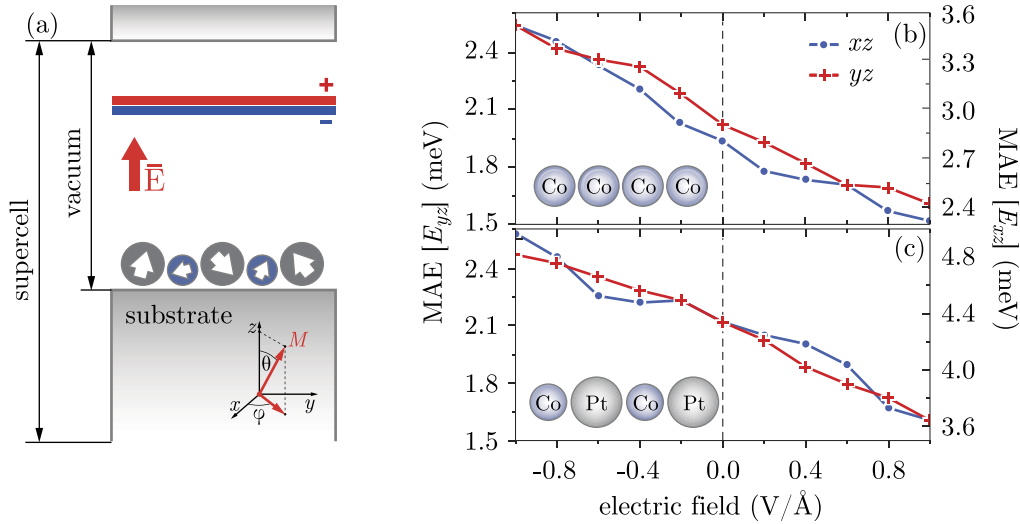


Figure 6. (a) Schematic diagrams of a unit cells for the calculation of the influence of EEF on the MAE of linear chains. The inset clarifies the use of angles in defining the direction of magnetization the magnetization (\vec{M}). (b), (c) The effect of the electric field on MAE of linear Co (b) and the mixed Co–Pt (c) chain. In both cases ((a) and (b)) E_x , E_y and E_z are intermediate, hard and easy axes, respectively. The red crosses represent MAE $_{yz}$ and blue circles stand for MAE $_{xz}$. (Adapted with permission from [63] copyright (2012) The American Physical Society).

including spin–orbit coupling. A static electric field was applied perpendicular to the surface and dipole corrections were taken into account [125]. For a linear chain on the surface, apart from the easy and hard axes, defined unambiguously, also intermediate magnetization axes can exist, defined by saddle points in the magnetization direction resolved energy landscape. In Co and Co–Pt chains on Pt(111) the easy axis is found to point along the z direction (out of plane), while x and y directions (in plane) take it in turns to be the hard and intermediate axes. In figures 6(b) and (c) both energy differences $\Delta E_{x(y)z} = E_{x(y)} - E_z$ are given.

The relative variation of the MAE (E_{yz}), as the electric field changes from 1.0 V/\AA to -1.0 V/\AA , is 67% and 57%, for the Co chain and the Co–Pt chain, respectively. Whereas E_{xz} increases by 34% and 39%, in the same electric field range. The change of MAE is as large as 1.2 meV/atom for the Co chain and 1.4 meV for the Co–Pt chain. The authors also argue that, extrapolating the results, one might expect higher electric fields to switch the easy axis to an in-plane direction.

The physical origin of the change in MAE is related to the spatial redistribution of the electronic density in response to the electric field, and the corresponding changes of the density of states near the Fermi energy. Figure 7(a) shows the density of states for the p orbital (majority and minority) of the Co atom in different EEFs. Spin-dependent changes of the LDOS at the Fermi level explain, via the second order perturbation theory [63], the preferred easy axis direction and the changes in the MAE [63].

Here also, the surface screening phenomena are found to be spin dependent [62], owing to the ferromagnetic nature of the material. The majority and minority p electrons screen the electric field differently, where the minority states show higher variation with the change of the electric field. Figure 7(b) [63] shows the difference in charge distributions

between the systems exposed to electric fields of opposite polarities ($\rho_{\uparrow(\downarrow)}^{-0.8 \text{ V/\AA}} - \rho_{\uparrow(\downarrow)}^{0.8 \text{ V/\AA}}$) for majority- and minority-spin channels. In this figure it is clearly shown that the effect of the EEF is stronger on the minority states than on the majority ones. It is associated with the screening by the delocalized p states (figure 7(a)), which in turn affects the d states of the Co atoms and alters the magnetic properties.

2.4. Tuning magnetic properties of thin films with external electric field and quantum well states

Another feature of low-dimensional structures making them an attractive subject for magnetic property manipulation is the quantum confinement often found therein [126–128]. The fact that quantum well states (QWSs) can have an influence on magnetic properties at the interface of the well is a well established one. For instance, a variation of magnetic properties has been observed in Co wires evolving from a single monoatomic chain to a 2D nanostructure [126]. An oscillatory magnetic anisotropy dependence was measured in Cu overlayers of varying thickness deposited on Co thin films, suggesting that the QWSs modulate the magnetic properties of the Cu/Co(001) interface [129]. Moreover, since electric field screening involves redistribution of the surface charge, it should obviously affect the boundary conditions of the QWSs, if the latter exist in the system. In particular, spin-polarized QWSs [130] are conceivably a good candidate for acting as a mediator between the electric field and magnetic properties of the system. As a particular example, it has been demonstrated that in magnetic tunneling junctions involving Fe thin films the contribution from the QWSs to the resonant tunneling through the iron films is significant [131].

While one might argue that quantum confinement is mostly associated with quasi-free (s-, p-like) electrons while

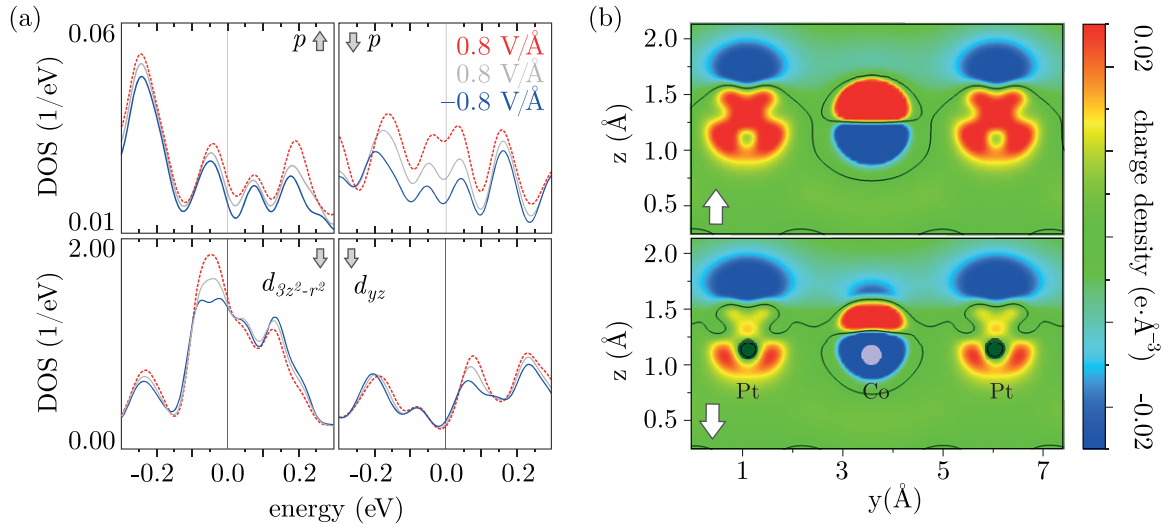


Figure 7. (a) The density for p states of a Co atom in the Co–Pt chain for spin up and spin down is presented in the upper panels. The lower panels show the orbital projected d-LDOS of a Co atom in the Co–Pt mixed chain for minority d_{xy} and $d_{3z^2-r^2}$ states. The gray line, full line and dashed line represent the density of states at -0.8 V/Å, 0.0 V/Å and 0.8 V/Å electric fields, respectively. (b) Cross section of the difference in the charge distribution at -0.8 and 0.8 V/Å for majority and minority states. The contour lines represent zero charge difference. The dimensions z and y represent the vertical and the horizontal coordinates of the cross subsection. (Adapted with permission from [63] copyright (2012) The American Physical Society).

magnetic properties are mostly determined by localized d electrons, the existence of d-QWSs has also recently been revealed [132, 133], along with their influence on MAE of layered systems. For instance, thickness-dependent spin-split dispersions for Co thin films on Mo(110) have been measured [134]. Further experimental studies on ferromagnetic Fe [135] and Co [136] films show an oscillatory uniaxial anisotropy having a period of a few monolayers.

2.4.1. Co(Fe) monolayers on Pt(001) surface. For Fe and Co monolayers on a Pt(001) surface covered by a Pt cap (see figure 8(a)), it was shown [63] that spin-polarized QWSs in the system can indeed be altered by EEF application. It is well known that FePt alloys have high magnetic anisotropy energy (~ 5 meV/Fe at.) [123]. For both Fe and Co monolayers the MAE has an approximately linear behavior with respect to EEF and the change of MAE is of the order of 0.2 meV per 1 V/Å, shown in figure 8(b). The same behavior for an Fe monolayer was also reported in other *ab initio* studies [123]. The curious fact that EEF seems to have opposite effects on Fe and Co monolayers is easily understood if one considers that EEF tends to favor in-plane magnetic anisotropy [63], thus positive electric field decreases the values of the MAE oriented out of plane (Fe) and increases the in-plane anisotropy (Co).

The mechanisms behind the phenomenon can be traced back to the overlap of 3d–5d orbitals (alloying of Fe(Co) atoms with Pt). Pt has high spin–orbit coupling, which has a significant impact on the magnetic properties of the compound. Hence, taking Co as an example, for Co layers in the Pt/Co_N/Pt(001) structure the external electric field affects the hybridization of Co and Pt, and such variation on the Co–Pt interface will change the magnetic properties of the film. Analysis of *ab initio* data [63] can yield information about the orbitals responsible for the screening of the external

electric field, and the variation of the magnetic properties. For instance, in figure 8(c) the density of states is plotted for different orbitals of Co and Pt that were found to be susceptible to EEF and involved in the process of screening of the latter. Other than surface dipole formation [137], the screening of the electric field directly involves s and p states of the capping Pt layer. This leads to the variation in the d orbitals of the Pt via sp–d hybridization, and the overlap among d orbitals of Co(Fe) and Pt will affect the magnetic properties [63]. Delocalized sp states of Co(Fe) are also involved. The changes of the MAE are again explained using the second order perturbation formalism [63].

An important factor therein is the change of the density of states around the Fermi level. It is exactly this change that links the EEF, QWSs and MAE. The EEF screening changes the electrostatic potential at the surface, changing also the confinement boundary conditions. As a consequence the energy positions of the QWS levels shift, with the levels closest to the Fermi energy moving in or out of the Fermi level area. As is illustrated in figure 8(c), this inevitably changes the LDOS at the Fermi level, leading, according to the second order perturbation theory, to a change in the preferred direction of the magnetization, i.e. of the anisotropy (figure 8(b)).

2.4.2. Fe multilayers on Pt(001) surface. To attain a more general conclusion, the authors of [63] studied the effect of EEF on the same system with varying number of Co(Fe) layers instead of a monolayer (Pt/Fe(Co)_N/Pt(001)).

The response of the MAE of a system with four Fe layers (Pt/Fe₄/Pt(001)) to the EEF is presented in figure 9(a). It has the same near-linear behavior as the system with just one Fe layer, though showing the opposite trend of increasing MAE with increasing positive EEF. Thus to get an overview of how the systems with different thicknesses of Fe react to

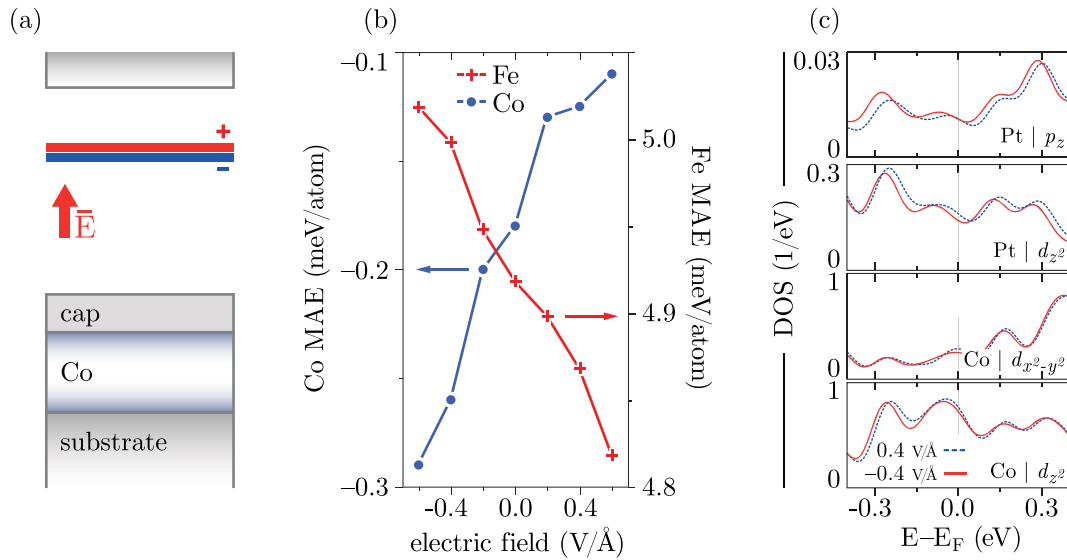


Figure 8. (a) The sketch of the calculation setup for Co mono- and multilayers on Pt(001). (b) The effect of the electric field on the MAE of Pt capped Co and Fe monolayers on the Pt(001) surface. (c) LDOS of the capping Pt and underlying Co layer under the influence of EEF of 0.4 V/Å (blue dashed) and -0.4 V/Å (red solid). (Adapted with permission from [63] copyright (2012) The American Physical Society).

the EEF, the authors, taking into account the linear behavior, quantify that reaction by the rate of change of the MAE ($\Delta E = [\text{MAE}(0.4 \text{ V/Å}) - \text{MAE}(-0.4 \text{ V/Å})]/[0.8 \text{ V/Å} \cdot \text{MAE}(0 \text{ V/Å})]$). In figure 9(b) this rate is presented as a function of the thickness of Fe. For all Fe layers, except for one layer of Fe, a negative electric field increases the MAE. The highest change rate is found for four layers of Fe.

To show that the mechanism of MAE change here is identical to the one discussed above for a single monolayer of Fe, i.e. the change of MAE can be associated with the influence of the EEF on QWSs, rather than with the pure contribution from the Fe–Pt interface anisotropy, in figure 9(c) the Kohn–Sham levels (close to the Fermi energy) which have non-zero occupancy are presented. The eigenenergies are plotted for EEFs of -0.4 V/Å and 0.4 V/Å (denoted as - and +, respectively). In figure 9(c) both the majority and minority states are shifted by an EEF, which resembles a Stark shift. Moreover, one can see that in the process of shifting some of the levels pass the Fermi energy, thus changing the Fermi level LDOS and, as discussed above, thus affecting the magnetic anisotropy.

Thus we see that the EEF can affect the magnetic moment and magnetic anisotropy of various surface structures, from sub-nanoscale ones to multilayer sandwich systems.

3. Surface charging with electrolytes

As has already been discussed in section 1, the strongest magneto-electric effect can be observed in materials where magnetic properties are predominantly governed by charge (electron or hole) carrier concentration [51, 66, 32, 138, 139, 12, 140]. Vivid examples of this flavor of magneto-electric coupling are ferromagnetic semiconductors [32, 51] and complex layered metal-oxide systems [138]. For instance, Ohno *et al* succeeded in controlling ferromagnetism in a

thin-film semiconductor alloy, where ferromagnetic exchange couplings between localized magnetic moments are mediated by valence-band holes [51]. The EF modifies the concentration of charge carriers, thus allowing one to tune the transition temperature of the hole-mediated ferromagnetic state. Here the carrier concentration is controlled by the field effect in a semiconductor–insulator–metal system.

In a purely metallic system, as we have seen in the previous section, the charge is provided by the metal itself in the attempt to screen the EEF. However, the charge density redistribution obtained in this manner is relatively moderate. One way to provide additional charge is to add to the surface a layer of an ionic liquid [140] or electrolyte [66].

3.1. Layered metallic systems

Weisheit *et al* have shown [66] that, immersing a highly magnetically anisotropic Fe/Pt or Fe/Pd layer in electrolyte (see figure 10 for a sketch of the experiment) and applying a bias across such a junction, one can reversibly modify the MAE of the system, as is evidenced by the change in the coercivity of the sample and the Kerr rotation angle (figures 11(a) and (b)). The electric double layer (EDL) formed at the interface in that case acted as a donor of charge carriers (electron or holes), thus enhancing the bare EEF screening of the metal. The experiment has been done on Pt and Pd based systems, in each case with two different thicknesses of the FePt or FePd films. The results presented in figure 11(a) show that thin layers are more susceptible to the carrier density change. This makes sense if one considers that the charge density redistribution and the associated anisotropy change are concentrated at the interface, leaving the bulk of the system unchanged. In the case of thinner slabs the interface anisotropy dominates the system, allowing for more drastic changes of MAE at the same bias voltages (electric field strengths).

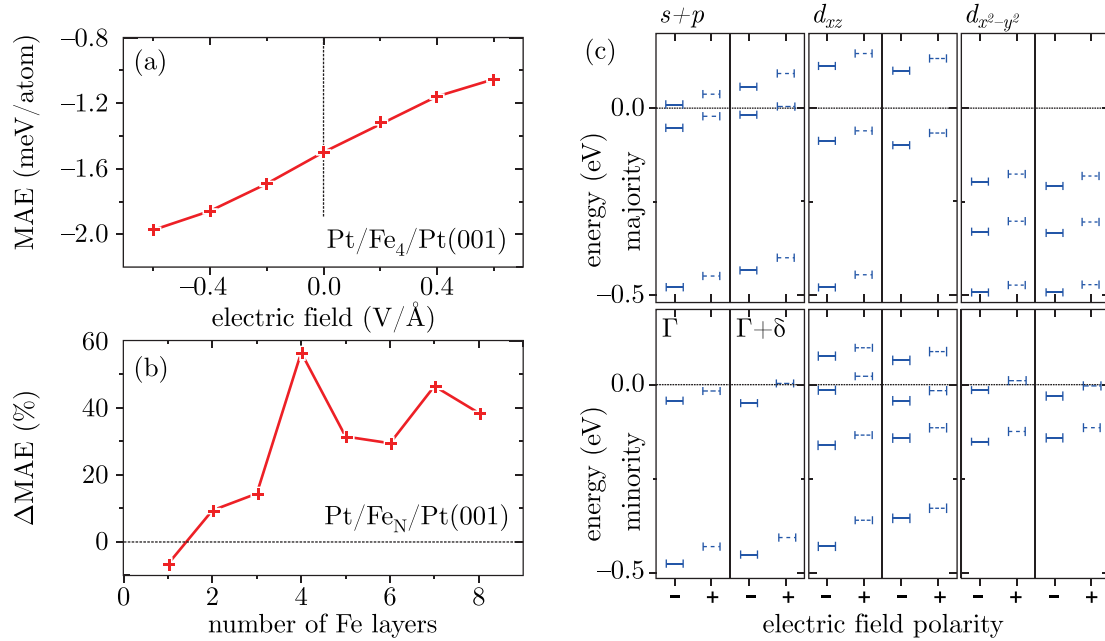


Figure 9. (a) The MAE as function of EEF for a Pt/Fe₄/Pt(001) supercell. (b) The rate of change of the MAE (Δ MAE), as a percentage, as a result of an EEF normalized by the MAE of the neutral system, for different numbers of Fe layers of the Pt/Fe_N/Pt(001) system. (c) The Kohn–Sham eigenenergies close to the Γ point for which the $s + p, d_{xz}$ and $d_{x^2-y^2}$ orbitals of four layers of Fe (Pt/Fe₄/Pt(001)) have high contributions. The energy of the electronic levels (relative to the Fermi energy) are presented for an electric field of 0.4 V/\AA (dashed lines) and -0.4 V/\AA (full lines), and two k -points, Γ and $\Gamma + \delta$ points, have been considered ($\delta = 0.03 \text{ 1/\AA}$). (Adapted with permission from [141] The American Physical Society, copyright 2013).

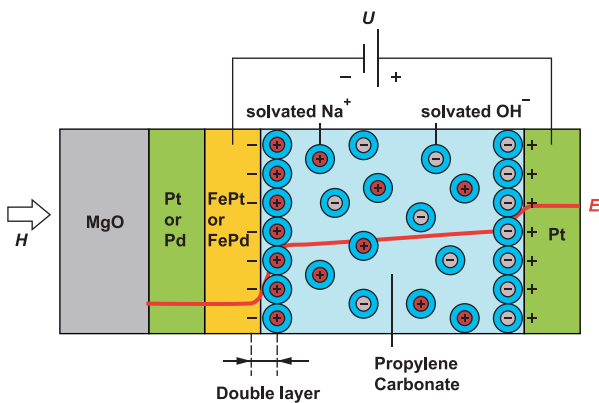


Figure 10. Schematic diagram of the electrolytic cell containing the FePt or FePd film within an applied magnetic field potential profile E due to the applied potential U indicated by the red line. The potential drop on the Pt electrode side is much lower (as compared to that of the sample surface) as a result of the Pt electrode’s large surface area. (Adapted with permission from [66] AAAS, copyright 2007).

A similar effect has been proven to exist on ultra-thin Co layers by Shimamura *et al* [140]. To enhance the effect of the applied EEF, Co layers have been coated with a polymer film containing an ionic liquid. The Curie temperature of the system was found to change by as much as 100 K upon application of an external bias of $\pm 2 \text{ V}$. With no bias applied, the T_C of the system was estimated to be $\sim 324 \text{ K}$, being much lower than the bulk value due to the two-dimensionality of the system [140]. Applying just a small bias (not exceeding 2 V)

to the sample at room temperature, the authors were able to open the magnetic hysteresis loop for the ultra-thin Co film, reenabling the magnetic anisotropy (see figure 12). At a bias of 2 V the T_C of the system could be enhanced to 380 K and the coercivity of the film reached 15 Oe .

The same ideas of using an EDL provided by an electrolyte to control the magnetism of monolayers can be applied to nano- and subnanoscale structures adsorbed or embedded into the surface (figures 13(a) and (b)). In fact, low-dimensional systems are even more susceptible to a change in the charge carrier density at the surface. Magnetic properties of single adatoms, clusters and cluster ensembles are predominantly dependent on the substrate-mediated exchange interaction. In metallic systems the latter usually has a Ruderman–Kittel–Kasuya–Yosida (RKKY) type [142–152, 121] and is highly sensitive to the electron or hole concentration. Very often magnetic interactions are mediated by surface state electrons, which are located precisely in the region where significant charge redistributions can be induced by external EFs or an EDL of an electrolyte. Despite the fact that these interactions are weak, of the order of a few millielectronvolts, they have a strong influence on the growth of nanostructures at low temperatures [145, 153, 154]. Previous theoretical investigations of the surface electronic structure of Cu(111) in the presence of EEF revealed interesting changes in the dispersion relation of the surface states, which involve modifications of the effective electron mass and Fermi wavevector (see also section 5) [74, 155, 75]. These results let one expect that surface charges and EFs should affect the scattering of impurities and, consequently, the interactions between them.

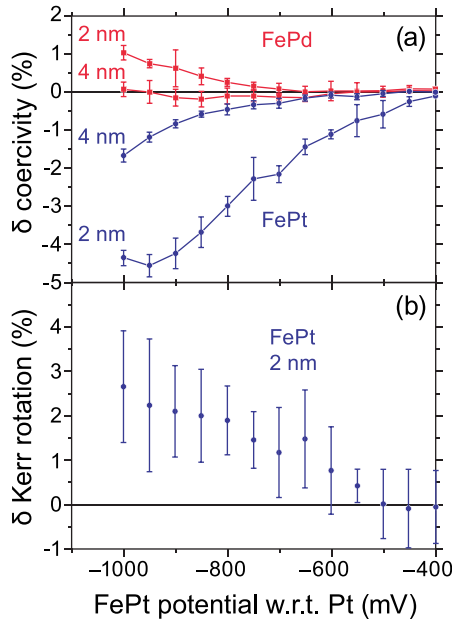


Figure 11. (a) Change of the film coercivity for FePt and FePd with external voltage at given thicknesses and (b) change of the Kerr rotation for the 2 nm thick FePt film with regard to the value at -400 mV. Error bars indicate the statistical variation (σ) of the measurements. (Adapted with permission from [66] AAAS, copyright 2007).

It is therefore rather interesting to explore the possibility of EF manipulation of interparticle magnetic interactions by tuning the surface electron density of a noble-metal surface by electrolyte-enhanced EEF.

By way of an example a theoretical study of the exchange interaction of substitutional surface impurities (Co and Fe) at a Cu(111) surface can be mentioned [67]. In this, the charge density accumulation on top of a Cu(111) surface was modeled by introducing an overlayer of point charges and magnetic properties of impurities at different surface charge concentrations were self-consistently determined. This model might seem a little crude, but it essentially captures the physics of the matter. The electric double layer formed at the interface between an electrolyte and a metal basically exposes the surface to the electrostatic potential of the interface ions (Stern layer), which can be modeled by point charges. This does, however, rely on the assumption that the adsorption position and charge/energy of the ions do not depend on the strength of the applied bias [156].

3.2. Single impurities

As a first informative example, the reaction of a single substitutional impurity [Co, Fe/Cu(111)] to the presence of a surface charge layer is shown in figure 13(c): more specifically, the dependence of the local magnetic moment of the impurity on the overlayer charge q . In the absence of an overlayer charge, the calculated magnetic moment of a substitutional Co impurity is $\mu_{Co} = 1.35 \mu_B$, while for a Fe impurity it is $\mu_{Fe} = 2.80 \mu_B$. These magnetic moments are largely affected by the EF generated by overlayer charges. For $q < 0$, the repulsive electrostatic potential pulls the electronic

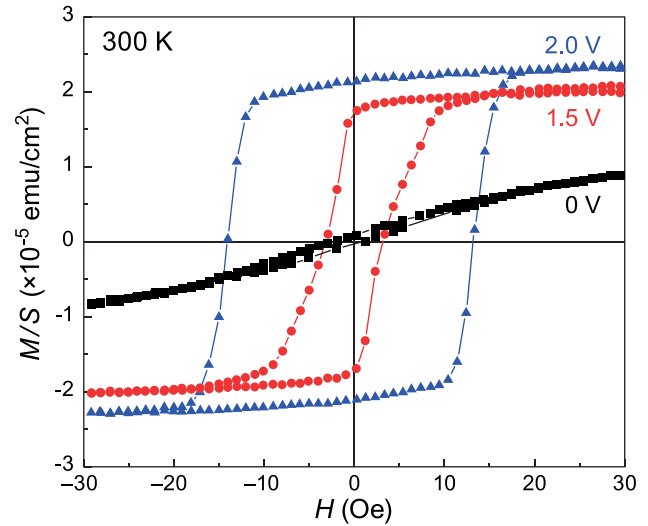


Figure 12. Magnetization (M) versus external magnetic field (H) curves at 300 K (of a Co layer supported on an MgO wafer and immersed in an ionic liquid contained in a polymeric film) under different gate voltages: 0, 1.5 and 2.0 V. The vertical axis represents M divided by the total area of the sample (S). VG was applied in an order of. H was applied perpendicular to the sample plane. (Adapted with permission from [140] American Institute of Physics Publishing, copyright 2012).

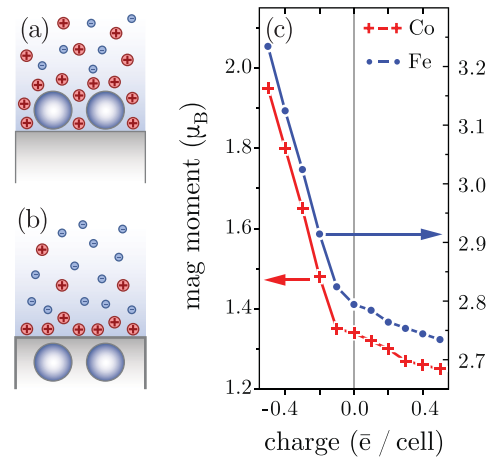


Figure 13. Calculated local magnetic moments at a single substitutional impurity as a function of overlayer charge q . The results for a Co (Fe) impurity are on the left (right) scale. (Adapted with permission from [67] The American Physical Society, copyright 2012).

charge away from the surface into the Cu bulk, causing a reduction of the number of electrons at the Co or Fe atom sites. This redistribution of charge density concerns mainly the higher-energy minority-spin states and therefore leads to the enhancement of the impurity magnetic moments. As $|q|$ increases ($q < 0$), a monotonic increase of μ_{Co} and μ_{Fe} is observed, reaching $\mu_{Co} = 1.95 \mu_B$ and $\mu_{Fe} = 3.24 \mu_B$ for $q = 0.5$ (figure 13(c)). For this value of q , the number of electrons at the impurity site is reduced by about 0.3–0.4 electrons, causing an enhancement of $0.6 \mu_B$ and $0.4 \mu_B$ in the magnetic moment of Co and Fe, respectively. A peculiar feature of the trend is that the slope of the $\mu_{Fe(Co)}(q)$ curve

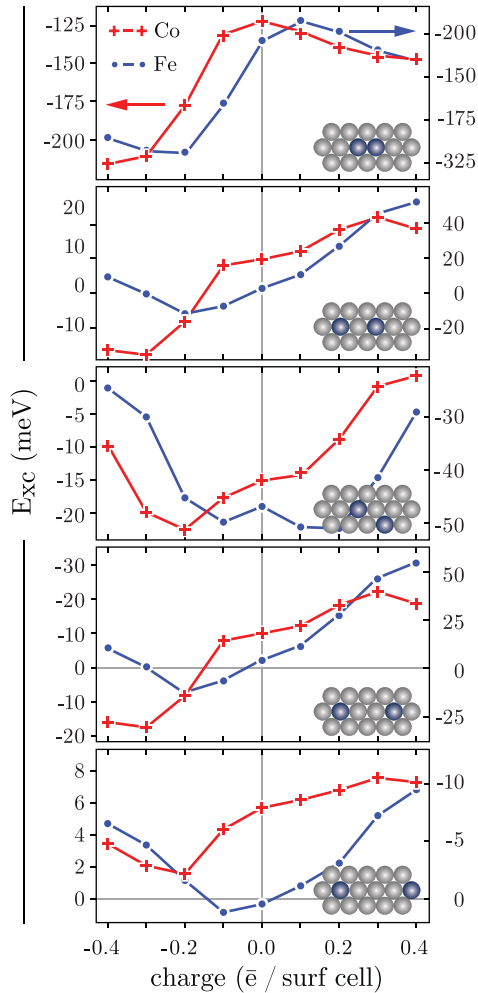


Figure 14. Exchange interaction energy of Co and Fe substitutional impurities at the Cu(111) surface as a function of the surface charge per atom q . Corresponding geometries are sketched as insets. (Adapted with permission from [67] The American Physical Society, copyright 2012).

is much larger for negative q than for positive ones. The explanation lies in the mobility of electrons and holes at the surface. The electron bath of the metal bulk provides a virtually unlimited capacity for accommodating electrons, which makes pushing them away from the surface an easy task. The remaining holes are highly local and do not constitute a problem. Increasing the electron density at the surface is, in contrast, linked to a drastic increase of the Coulomb repulsion energy, making the slope of the $\mu_{\text{Fe(Co)}}(q)$ curve in figure 13(c) much smaller for positive q .

Another interesting feature is the kink in the curves at small negative q , while one might naively expect it to be exactly at zero. The reason for the generally weak effect of small values of negatively charged ions on the surface atoms is presumably related to the natural spill-out of the surface electron density into the vacuum. In fact, in a neutral system, about 0.2 electrons per atom are found in the volume outside the atomic spheres of the surface atoms. These are basically the electrons that are displaced in order to screen the EF for small q . Consequently, the orbital occupations at an embedded impurity are not as strongly affected. It is only for larger

values of $|q|$ that a significant electron-density depletion at the impurity occurs.

3.3. Impurity pair interaction

It is obvious that the exchange interaction between substitutional impurities will also be susceptible to the influence of the EEF induced by the charge layer at the surface. Moreover, the effect will originate from two physical effects: the change of the local magnetic moments of the impurity atoms will have a direct influence on the exchange interaction, but also the change of electron density in the substrate will play a role. For impurities residing further apart than first or second nearest neighbors, the exchange interaction is mediated by substrate electrons [147], whose density is highly susceptible to EEF or the surface charge layer. Figure 14 shows the effective exchange interaction energy $E_{\text{exc}} = E_{\text{FM}} - E_{\text{AFM}}$ between two Co(Fe) impurities as a function of the overlayer charge for different Co–Co separation distances (illustrated in the insets). Negative (positive) values of E_{exc} imply that an FM (AF) alignment of the impurity moments is favored.

If we trace the exchange in the absence of additional charge (i.e. different panels of the plot at $|q| = 0$) we shall see that the values for both Co and Fe rapidly decay, though not in a monotonic way, but rather in an oscillatory pattern. This is the classical RKKY interaction mediated by both bulk [142, 143, 145] and surface [157] electrons. The observed oscillation wavelength (2.5 Å [67]) hereby lies in between the values of bulk and surface state Fermi wavelengths (1.7 and 14.5 Å respectively).

The dependence on q for both Co and Fe is comparable, although $|E_{\text{exc}}|$ is, in general, stronger for Fe due to its larger magnetic moment. In the case of nearest neighbor (NN) positions of impurities (top panel in figure 14), the direct electronic hybridization of the impurities is very strong and dominates their interaction. Consequently, the absolute values of E_{exc} are around an order of magnitude larger than for any other impurity pair. Nevertheless, the overlayer charge affects significantly the magnetic exchange since it controls the displacement of electronic density around the impurities, thus modifying the orbital occupations near the Fermi energy and the transition metal (TM) atoms' hybridizations.

In the nearest neighbor configuration the effect of the surface charge can be understood from the density of d-electron states (DOS), reflecting the direct hybridization properties of the dimer. The DOS at a Co atom in a ferromagnetic NN dimer is shown in figure 15 for negative (a) and positive (b) surface charges of $\pm 0.3 \bar{e}/\text{cell}$. Here, one observes that for $q < 0$ the majority-spin states are shifted towards lower energies, compared to the neutral case (dotted line). At the same time, the minority-spin band is enhanced in intensity and shifted towards higher energies. This band displays a splitting into bonding and anti-bonding orbitals [103], for which the level rearrangements occur in a different way. The bonding orbitals located at lower energies suffer a stronger shift of about 0.6 eV, while the anti-bonding states shift by about 0.3 eV. Nevertheless, the smaller change in the position of the anti-bonding subband suffices for it to cross the

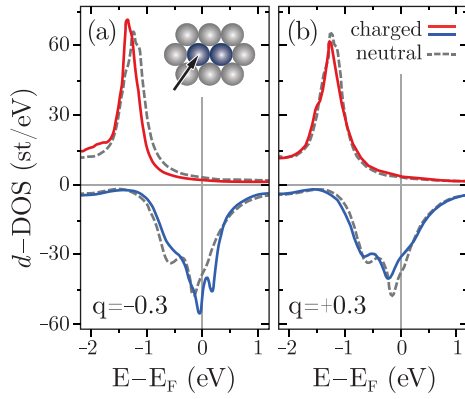


Figure 15. Local d-electron DOS at a Co impurity in a nearest neighbor dimer configuration. Results are given for overlayer charges (a) $q = -0.3 \bar{e}$ and (b) $q = +0.3 \bar{e}$. The corresponding DOS of the neutral system ($q = 0$) is given by dashed curves for the sake of comparison. (Adapted with permission from [67] The American Physical Society, copyright 2012).

Fermi energy and become unoccupied. Moreover, the opposite shifts of the majority- and minority-spin bands increase the magnetic exchange splitting, thus explaining the enhancement of the local magnetic moment. For $q > 0$, the majority- and minority-spin bands show a slight displacement towards lower energies and a decrease of intensity. These changes in the DOS are related to the enhancement of $|E_{\text{int}}|$ found for $q > 0$. Notice that the FM bonding and anti-bonding orbitals are similarly affected. Here, the local magnetic moments are not significantly modified.

At larger interimpurity distances r (e.g., for second-NN impurity positions and beyond) the direct electronic hybridizations between the impurities are no longer relevant. The local magnetic moments at the TM atoms approach the single-impurity values as displayed in figure 13(b). They are essentially the same in the FM and AF configurations. At second- and third-NN positions, the key role is played by the surface Cu atoms located between the impurities. In the second panel from the top in figure 14, results are given for E_{exc} between second NN Co and Fe impurities as a function of the overlayer charge. For $q < 0$ one observes that the FM coupling is preserved and even slightly enhanced by small values of $|q|$. See, for example, the results for $q = 0.1 \bar{e}$ and $0.2 \bar{e}$ for Co pairs and $q = 0.1 \bar{e}$ for Fe pairs. However, a remarkable non-monotonic dependence of E_{exc} on q is observed for larger $|q|$. The initial decrease of E_{exc} is followed by a rapid increase for stronger negative surface charges, which implies a strong destabilization of the FM state. The changes in E_{exc} are of the order of 20 meV (30 meV) for Co (Fe) impurities. Positive overlayer charges $q > 0.2 \bar{e}$ also tend to reduce the strength of the FM coupling. All in all, for the second-NN dimer geometry, both overlayer charge polarities preserve the FM alignment of the impurities ($E_{\text{exc}} < 0$), although the strength of the effective exchange coupling $|E_{\text{exc}}|$ is drastically reduced for $|q| > 0.3$. In contrast, for impurities at third-NN positions negative overlayer charges destabilize the AF alignment and lead to a switching of the magnetic coupling. On the other

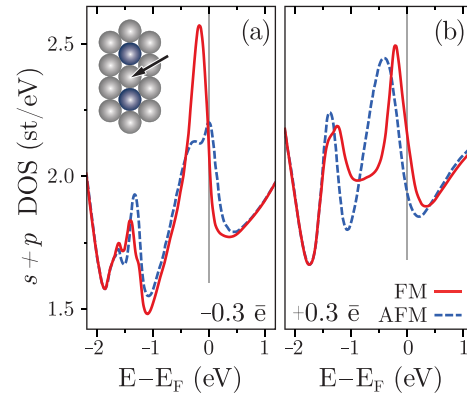


Figure 16. Local s- and p-electron density of states at the Cu atom located between two Co third-NN impurities. Results are given for overlayer charges (a) $q = -0.3 \bar{e}$ and (b) $q = +0.3 \bar{e}$. (Adapted with permission from [67] The American Physical Society, copyright 2012).

hand, for $q > 0$ the AF coupling is enhanced by about 10 meV for Co and by 40 meV for Fe.

At the second- and third-NN distances, the change in the total energy is dominated by the single-particle (SP) contribution $\text{ESP} = \int^{\epsilon_F} \eta(\epsilon)(\epsilon - \epsilon_F) d\epsilon$, where $\eta(\epsilon)$ is the electronic DOS [158]. Consequently, the magnetic exchange energy is determined by the differences in the DOS between the two magnetic configurations. However, already at second-NN distances, the local DOS at the impurity sites is not significantly affected by their relative alignment. Instead, the change in the local DOS at the Cu atoms located between the impurities plays the major role. Appreciable changes in the electronic structure are, in fact, induced at these atoms by the proximity with the TM impurities. In figure 16 the local density of s and p states at the Cu atom located between two third-NN Co impurities is shown. The curves are displayed for the FM and AFM alignments between impurities for $q = -0.3 \bar{e}$ and $+0.3 \bar{e}$. One observes that for $q = 0.3 \bar{e}$ the main peak in the DOS of the Cu atom between AF impurities lies at lower energies than in the case of a FM alignment (figure 16(b)). Therefore, according to the single-particle picture, an AF coupling is stabilized. This result is in agreement with the AF coupling found for $q = 0$. For $q = -0.3$ this peak is shifted towards higher energies (see figure 16(a)). A substantial decrease of intensity is observed, reducing the SP contribution by a magnitude proportional to the locally integrated change in the density of states. As a consequence, the AF alignment is destabilized, and the magnetic coupling between impurities switches to FM ($q < 0$).

While the q dependences of E_{exc} for first-, second-, and third-NN distances are quite distinctive, the behaviors at larger distances show some similarities (see lower panels of figure 14). This suggests that the q dependence of E_{exc} is the result of the same microscopic mechanism, namely, a modification of the delocalized electronic density at the Cu surface. In fact, for negative values of q , the electronic density at these Cu atoms is reduced by up to 0.3 electrons for $q = 0.4$, while for positive q it remains essentially unchanged. These

important changes in the electronic density are responsible for the distinctive q dependence of E_{exc} at larger distances.

Thus the EEF produced by an overlayer charge accumulation at the Cu(111) surface modifies the local magnetic properties and the interactions of surface substitutional magnetic impurities. The responses of Co and Fe impurities to external surface charging were found to be very similar [67]. Surface charging induces a displacement of electronic density at the impurity sites, which is mainly of minority-spin character. This charge redistribution causes large modifications of the impurity local magnetic moments. Moreover, three different microscopic mechanisms have been identified to cause the changes in the magnetic exchange E_{exc} between atomic impurities. In the case of NN impurities, the depletion of electronic density induced by the EF at the impurity sites strongly affects the direct electronic hybridizations which determine the exchange coupling. At second- and third-NN positions on Cu(111), the electronic structures at the impurity sites are not significantly affected by the relative orientation of the impurity moments. Instead, the Cu atoms located between the impurities play the central role. The EF induces changes in the local electronic structure of these Cu atoms, which cause important variations of E_{exc} including the switching from FM to AF alignment of the impurities and vice versa. At larger distances, beyond fourth NNs, the strength of the substrate-mediated RKKY interaction can be modified by the order of 10 meV. These modifications arise from the EF-induced changes in the delocalized electronic density at the Cu surface and in the scattering of the surface states at the magnetic impurities. Moreover, it has been shown that E_{exc} often displays a non-monotonic dependence on the overlayer charge, which implies drastic changes in the magnetic order. In this context, a contrasting behavior of the metallic screening has been found depending on the polarity of the external surface charges [67].

4. Direct surface charging: control of MAE and exchange interaction

Up to now, we have seen that EEF and electrolytes/ionic liquids can be used to affect magnetic properties of thin films and nanostructures on metallic surfaces. The underlying mechanism in most cases is the change of local charge carrier concentration caused by the EEF or electrolyte. An important role thereby has been played by the metal bulk supporting the system, which acted as a virtually infinite bath supplying or accommodating electrons or holes to or from the surface [64, 67, 63].

EEF and electrolyte are, however, by far not the only way to alter the charge and spin carried density at the surface. Another viable option is to use, instead of bulk metal systems, thin metal slabs or quantum dots supported on an insulator, effectively creating a charge trap [160–162, 159, 163, 68]. It has been shown that in such a charge trap, mostly based on graphene or metal–non-metal alloys, charge can govern mechanical [160], transport [161] and electronic [162] properties. For a monolayer of Fe adsorbed on graphene [159] it was shown that the MAE of Fe atoms strongly depends on

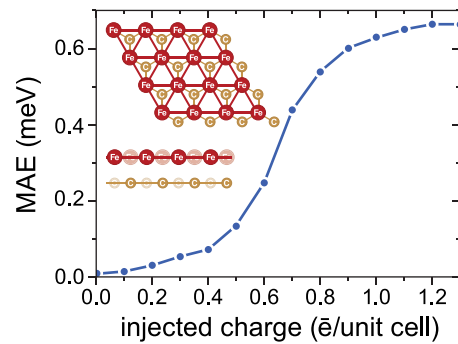


Figure 17. Dependence of the MAE of a Fe monolayer adsorbed on a sheet of graphene on the injected charge. (Adapted with permission from [159] American Institute of Physics Publishing, copyright 2012).

the amount of charge injected into the system (see figure 17). A most vivid example of how a small amount of additional charge can abruptly change the magnetic properties of the system is Pd. Being close to the Stoner instability [98], Pd is very susceptible to the change of electron density of states at the Fermi level. For example, theoretical calculations [163] predict that Pd multilayers can be switched between ferro- and paramagnetic states by charge injection.

Nowadays multiple experimental methods exist to achieve local charge injection, for example scanning probe microscopy [164–166]. As a choice of material for the system to use those methods on, slabs or nanoclusters of 3d–5d element alloys spring to mind. The 3d elements usually display small MAEs due to their reduced spin–orbit couplings (SOCs); however, the 4d–5d elements, which are paramagnetic but highly polarizable, have larger SOC. Thus, a significant enhancement of MAE is usually observed upon alloying between these two atomic species, making them a good starting point for devising a way to tailor magnetic properties by directly charging the system.

As a particular example of such a 3d–5d compound, Fe–Pt and Fe–Pd alloys are worth mentioning. They are already widely known for their technological applications such as magnetic recording design, owing to high Curie temperature ($T_C = 750$ K), saturation magnetization (1.4 T) and magnetocrystalline anisotropy constant ($K_u = 6.6$ MJ m $^{-3}$) [66]. For instance, first principles calculations on Pt–Fe ultra-thin films report anisotropy energy values of ~ 5 meV/magnetic atom [123].

In an *ab initio* study, Ruiz-Díaz and coworkers have systematically studied the effects of surface charge-doping on the magnetic anisotropy in free-standing 3d–5d multilayers, taking as a representative examples Fe–Pt layer-wise alloys adsorbed on a ten monolayer (ML) thick Pt(100) slab [68].

To rule out the possibility that charging can have an indirect effect on magnetic properties of metallic multilayers via electrostrictive relaxations in the system, the influence of excess electron (positive doping) or hole (negative doping) charge on the geometry of Fe–Pt slabs was studied [68]. In general, it was found that, for all Fe–Pt multilayer samples, the effect of the charge injection has, as a result, a modest interlayer expansion (no more than 2%) of the two outermost layers of the slab for both positive and negative doping, resulting thus in a non-appreciable change in MAE.

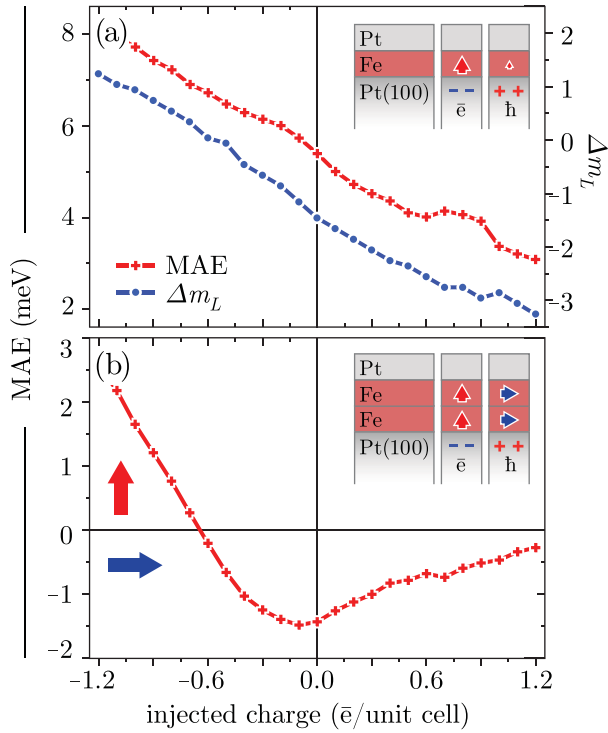


Figure 18. Calculated magnetic anisotropy energy (in meV/magnetic atom) for Fe–Pt multilayers as a function of the injected charge (holes) for (a) Pt–Fe–Pt(100) and (b) Pt/Fe₂/Pt(100). The charge-doping scale (in units of \bar{e} /unit cell) is referred to the neutral system. Positive (negative) values stand for an excess (lack) of valence electrons. Positive (negative) MAE values stand for an out-of-plane (in-plane) axis of magnetization. (Adapted with permission from [68] The American Physical Society, copyright 2013).

4.1. Fe–Pt multilayers

The influence of charging on the magnetic anisotropy of Fe–Pt layers is illustrated in figure 18. The value of MAE as a function of excess charge added to the system ($MAE(q)$) for a simple alloy system—one monolayer of Fe on Pt(001) capped with one more Pt monolayer—is shown in figure 18(a). It has been reported that this particular system exhibits a relatively large MAE (5.12 meV/Fe atom) having an out-of-plane axis of magnetization [123] and an enhancement of MAE by $\sim 13\%$ in the presence of an EEF [123, 167]. In full agreement with these studies, Ruiz-Díaz *et al* report an MAE value of 5.4 meV/mag. at. for a neutral system having an out-of-plane axis of magnetization (figure 18(a)). MAE follows a linear trend with respect to the charge-doping strength, which has been observed in the presence of EEF, yet the direct charge-doping was found to have a much stronger effect on MAE than external fields. A remarkable MAE enhancement of nearly $\sim 65\%$ (8 meV/mag. at.) is found for hole-doping of about $1.2 \bar{h}$ /cell, while a considerable reduction of $\sim 40\%$ (3 meV/mag. at. at $1.2 \bar{e}$) after electron-doping is observed with respect to the neutral system. These variations represent a net change of $\sim 95\%$, which is of the order of MAE for the neutral system itself.

The origin of such intensive change of MAE is the charge redistribution within the Fe–Pt slab. The charge introduced

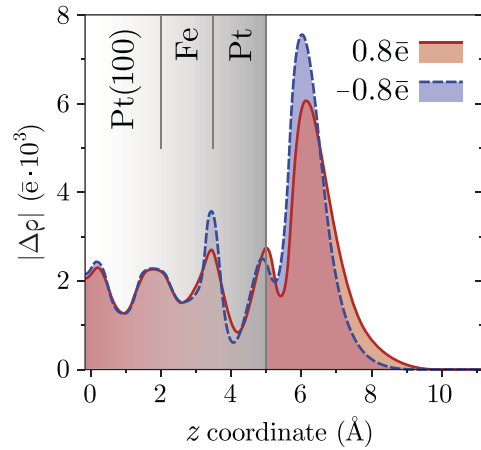


Figure 19. Plane-averaged charge density change (absolute value) due to electron- (red solid curve) and hole-doping (dashed curve) of Pt–Fe–Pt(100).

into the system is pushed by coulomb repulsion towards the interfaces, creating an additional cushion of charge above the surface and changing the charge carrier concentration in the surface region of the slab. As an example, the change of the plane-averaged charge density ($|\Delta\rho| = \rho(q) - \rho(q=0)$) induced by electron or hole injection in the system discussed above (Pt/Fe/Pt(100)) is plotted in figure 19. While the charge redistribution is strongest in vacuum above the surface, it is also sizable in the interstitial regions of the Fe–Pt interface and is bound to affect the Fe–Pt bonding. Moreover, since the 3d–5d hybridization is a key factor determining the anisotropy of the system, slab charging can be expected to have a strong effect of the MAE value or even sign.

The linear dependence of the MAE on the amount of injected charge, though common to quite a few systems, is, however, not a universal law. For instance, $MAE(q)$ for Pt/Fe₂/Pt(100) is shown in figure 18(b), exhibiting a clearly non-linear behavior. At zero charge, MAE has a near-minimum value (~ 1.5 meV/mag. at., having an out-of-plane axis of magnetization). Upon electron charging, MAE weakens to about -0.3 meV/mag. at. for excess charge of $1.2 \bar{e}$ per unit cell. Upon hole injection, MAE drops to zero for 0.6 holes and then, changing the sign, grows to as much as 2.5 meV/mag. at. for charges of 1.2 holes. The observed MAE behavior is the result of the interplay between the charge-doping and the existing strong spin–orbit interaction at the interface. Finding a simple explanation for this trend is not straightforward. However, further insights about the effects of the charge-doping on MAE can be inferred from other geometric and stoichiometric combinations of FePt multilayers.

4.2. Spin and orbital moments of Fe–Pt multilayers

Although the behavior of MAE under excess charge seems to be somewhat unpredictable, it can be analyzed and understood by studying the local magnetic behavior of the Fe–Pt multilayers and the spin and orbital moments of Fe and neighboring Pt layers. Spin and orbital moments for the two above compositions of Fe–Pt multilayers are illustrated in

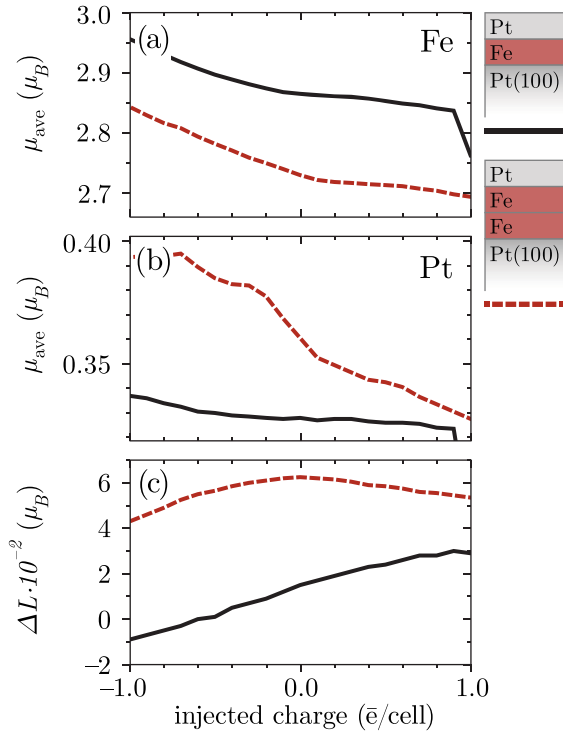


Figure 20. (a), (b) Average spin and orbital moments of the Fe (a) and the capping Pt (b) in μ_B . (c) Orbital difference ($\mu_L^z - \mu_L^x$) between out-of-plane and in-plane axes of magnetization (in $10^{-2} \mu_B$). The solid black and dashed red lines correspond to Pt/Fe/Pt(100) and Pt/Fe₂/Pt(100) respectively. (Adapted with permission from [68] The American Physical Society, copyright 2013).

figure 20. In the hole-doping regime, it is found that the magnetic layers can reach spin moments close to the bulk saturation value ($3.2 \mu_B$ assuming the bulk Fe d-band filling of $6.8 \bar{e}$) [68]. When electron-doping is increased, a decrease of the magnetic moment is observed. This is due to the reduction of the exchange splitting between majority and minority states caused by the excess of electron charge. Concerning the average spin moment of non-magnetic layers at the interface, a high induced polarization is observed. Pt layers in direct contact with Fe can be magnetized to up to $0.45 \mu_B$ on average. Pt develops the highest induced moment if it caps the multilayer, e.g. Pt/Fe_(1,2)/Pt(100). Other capping compositions display smaller magnetic moments, $\sim 0.25\text{--}0.45 \mu_B$ (according to our calculations, not presented here). Further, a smooth and monotonic reduction of the magnetic moment is observed when the number of electrons in the unit cell is increased. The variations of the spin moments reflect the charge-doping influence in the multilayers, but due to their robustness it is not so straightforward to follow their relation with more subtle quantities such as MAE.

4.3. Electronic structure analysis: decomposed density of states

The origin of the MAE behavior found in the Fe–Pt multilayers can also be investigated from a local perspective by analyzing the d-orbital-resolved LDOS of the magnetic layers for the

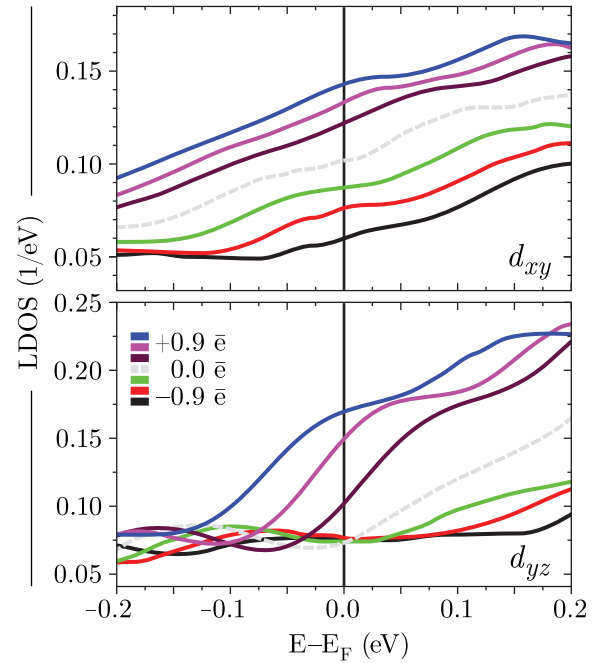


Figure 21. Decomposed minority d-orbital LDOS of Fe in Pt/Fe/Pt(001). (Adapted with permission from [68] The American Physical Society, copyright 2013).

same representative Fe–Pt capping compositions through the second order perturbation formula [168]:

$$\text{MAE} = E_x - E_z \sim \xi^2 \sum_{\text{o,u}} \frac{\langle \psi_{\text{u}} | l_z | \psi_{\text{o}} \rangle^2 - \langle \psi_{\text{u}} | l_x | \psi_{\text{o}} \rangle^2}{\epsilon_{\text{u}} - \epsilon_{\text{o}}} \quad (1)$$

where $\{\psi_{\text{o}}, \psi_{\text{u}}\}$ stand for the occupied and unoccupied states and $\{l_x, l_z\}$ are the angular momentum operators. The ξ parameter is an average of the SOC coefficients. Clearly, due to the denominator of the equation, the most dominant contributions to MAE come from the states close to the Fermi level. Further, ignoring the spin-flip terms between up and down states, the main changes in MAE can be only attributed to the coupling between states in the minority band. Then, after an analysis of the spin–orbit coupling matrix elements between different d orbitals, MAE trends can be qualitatively inferred. As an example, the Pt/Fe/Pt(100) system is discussed.

In figure 21 the d-orbital-resolved LDOS for the minority band is plotted. Since the majority LDOS is fully occupied and featureless around the Fermi level, it is not expected to have an effect on MAE and is thus neither plotted nor discussed. In the case of Pt/Fe/Pt(100) it is found that the MAE trend presented in figure 18(a) is mainly governed by the coupling between the d_{xy} and d_{yz} orbitals, and the observed linear behavior can be explained. First, such coupling favors an out-of-plane direction of magnetization. Second, the d_{xy} orbitals undergo a monotonic depletion near the Fermi level upon hole-doping, reducing the contribution of the first term of equation (1) to MAE. Thus, this reduction enhances MAE in the hole regime.

We can see that MAE trends in metallic multilayers can be explained, to a large extent, through the second order perturbation formula. The most dominant couplings, favoring a particular direction of magnetization, determine the direction of the easy axis.

4.4. Relationship between MAE and orbital anisotropy

Another way to understand the change of MAE in the system is to follow the relationship between MAE and the orbital moments in magnetic films, in particular in 3d ultra-thin films. This correspondence is known as Bruno’s relation [169]. The approach lies in the analysis of the variation of orbital moments (also called orbital anisotropy) between two quantization axes. As an example, the out-of-plane and the in-plane directions of magnetization of the Fe layers can be taken (z and x direction respectively). The orbital moment anisotropy (OMA) does not follow a simple gradual depletion if the number of electrons is increased, but a more complex non-linear behavior (see figure 20(c)).

For magnetic ultra-thin films, Bruno’s relation can be formalized as follows: $\Delta E_{\text{SOC}} = -\frac{\xi_{\text{Fe}}}{4\mu_B} \Delta m_{L,\text{Fe}}$, which assumes a direct correspondence between OMA and MAE. Experimental evidence along with the second order perturbation theory and first principles calculations [170] suggest that Bruno’s formula is often, yet without claim to unconditional generality, valid for systems where only the on-site contributions to MAE are significant and the exchange splitting is large enough. Apart from this, if the hybridizations are not negligible and the spin-flip terms are important, as in the case of strong SOCs, it is not expected to find a simple correspondence between MAE and OMA, and a more general relationship between MAE and OMA needs to be employed [170].

Here we shall only give one example of how Bruno’s formula can be applied for charged systems, even though the formalism was developed in the framework of neutral ones (see figure 22). Here a clear near-linear trend can be found linking MAE and OMA throughout the whole excess charge range ($-1.2\bar{e}$ to $+1.2\bar{e}$). Analysis of multiple other possible Fe/Pt layer-wise alloy samples (not presented here) has shown that, e.g., Pt/Fe/Pt(100) and Pt/Fe/Pt/Fe/Pt(100) fulfil the Bruno relation. They are, however, part of the minority of configurations that strictly follow the relation. Other capping compositions only partially comply with it. For some of the considered Fe–Pt multilayers, a completely non-linear dependence between OMA and MAE was observed, showing that in some cases hybridizations along with the strong SOCs of the Pt layers are strong enough and cannot be tuned by charge-doping injection.

5. Surface electron polarization controlled by electron confinement and electric field

Up to now we have been discussing the possibilities to control spin magnetic moments of metallic nanostructures with non-magnetic means, more specifically with electric fields and surface charging. Yet sometimes the spin-polarization of free of quasi-free electrons is also a stable observable quantity, which can also be interesting from fundamental and applied points of view. As an example, we shall take a look at the effect of the electric field on the band structure and local polarization of metallic Shockley surface state electrons [171, 172, 74, 75] confined to a single nanostructure [173, 73, 174].

The key concept here is using EEF for sample band structure manipulation, a cornerstone concept in modern electronics

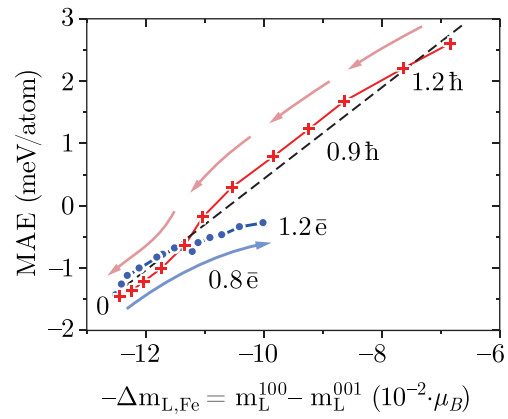


Figure 22. Relationship between magnetic anisotropy (MAE) and orbital moment anisotropy (OMA) of the Pt/Fe₂/Pt(100) system. (Adapted with permission from [68] The American Physical Society, copyright 2013).

technology. Desired effects (logic element switching in most cases) are usually achieved by altering electrostatic potentials in multi-terminal devices through applying bias voltages to the gate terminals [175]. Thereby, the quantity of interest that is to be manipulated is, for the vast variety of spintronic devices and their prototypes, the magnetoresistance [176], which describes the dependence of the current through a sandwich junction (I) made of two magnetic layers interspaced with a para- or diamagnetic separator on the mutual magnetization orientation of the magnetic leads ($\uparrow\uparrow$ or $\uparrow\downarrow$) [176–178]. The measure of this dependence is the tunneling magnetoresistance ratio (TMR) defined as [179]

$$\text{TMR} = \frac{I_{\uparrow\uparrow} - I_{\uparrow\downarrow}}{I_{\uparrow\downarrow}}. \quad (2)$$

This ratio is usually defined by the junction geometry and is thus fixed at construction/assembly time. The magnetization reversal (information recording) of one of the magnetic leads can then be achieved in a conventional way, i.e. by applying a magnetic field or a spin torque current to the junction. Either way, it is a rather energy intensive process and finding a more effective way of switching the polarization (or, for that matter, changing the TMR altogether) is a rather lucrative venture. This is where the idea of using EEF (without an electric current) to control the TMR comes in.

5.1. Surface states and local magnetic properties

Ignatiev *et al* have proposed, using *ab initio* calculations to support the arguments, to use the fundamental possibility of locally controlling the TMR with two basic effects: (i) band structure manipulation through application of the EEF [74, 62, 180, 99, 100, 123, 181] and (ii) the spatial confinement of a quasi-free two-dimensional electron gas (2DEG) to a closed geometry (e.g. that of a nanoisland) [182, 73, 174]. As a test subject a well established model system of a bilayer Co island [183, 184] on a Cu(111) surface was taken [185, 182, 73, 174].

In spin-polarized STM experiments the actual spin-polarization of the sample is usually determined or approximated from the asymmetry of the differential conductance $\frac{dI}{dV}$ at parallel $\uparrow\uparrow$ and antiparallel $\uparrow\downarrow$ alignments of tip and sample magnetizations [176, 73].

$$A = \frac{\frac{dI}{dV}_{\downarrow\uparrow} - \frac{dI}{dV}_{\uparrow\uparrow}}{\frac{dI}{dV}_{\downarrow\uparrow} + \frac{dI}{dV}_{\uparrow\uparrow}}. \quad (3)$$

Using the theory of Tersoff and Hamann [186, 187] generalized for the magnetic case [188–190], the differential conductance $\frac{dI}{dV}$ can be rewritten as

$$\frac{dI}{dV} \propto n_T n_S + \vec{m}_T \cdot \vec{m}_S, \quad (4)$$

where n_T and n_S are the density of electronic states of the tip and the density of states created by the sample at the position of the tip, respectively, and \vec{m}_T and \vec{m}_S are defined in terms of local spin-polarizations as

$$\vec{m} = (n_{\uparrow} - n_{\downarrow}) \vec{\mu} = (n_{\uparrow} + n_{\downarrow}) P \vec{\mu}, \quad (5)$$

$\vec{\mu}$ being a unit vector defining the direction of the spin moment and P being the local spin-polarization, defined as

$$P = \frac{n_{\uparrow} - n_{\downarrow}}{n_{\uparrow} + n_{\downarrow}}. \quad (6)$$

Combining all together, the following expression is obtained:

$$A \propto -P_S P_T, \quad (7)$$

where P_S and P_T are the polarizations of the sample and the tip, respectively. It should be noted that all the values mentioned above are understood to be energy-dependent quantities, so that, e.g., $n_{\uparrow(\downarrow)} = n_{\uparrow(\downarrow)}(E)$ and $P = P(E)$.

In the same manner polarizations P_S and P_T can be related to the TMR. Indeed, according to the Julliere formalism [176], the tunneling current can be written as

$$I(E) = I_0(E) (1 + P_T(E) P_S(E) \vec{\mu}_T \cdot \vec{\mu}_S). \quad (8)$$

Using this formula in equation (2) one easily obtains for TMR

$$\text{TMR}(E) = \frac{2 P_T(E) P_S(E)}{1 - P_T(E) P_S(E)}. \quad (9)$$

Polarizations of the tip and the surface states are of the order of 10–20%. This means that $|P_T P_S| \ll 1$ and allows one to estimate the TMR behavior by expanding (9) in a Taylor series of $\Pi(E) = P_T P_S(E)$. If one further assumes that the polarization of the tip remains largely unchanged ($P_T \equiv \text{const}$), we get

$$\text{TMR}(E) \simeq 2\Pi(E) + O(\Pi^2(E)) \simeq P_S(E) + O(P_S^2(E)). \quad (10)$$

This means that, at small tip and sample polarizations, the TMR is proportional to the STS spin-asymmetry with an opposite sign. Thus the TMR can be estimated from the polarizations of the tip and the surface¹ alone. This conclusion was recently confirmed by two STS experiments performed on bilayer Co islands grown on Cu(111) [73, 174]. In the following, for the sake of simplicity, the polarization of the tip of 20% will be used as an estimate.

¹ To be precise, from the spin-polarized DOS of the surface at the position of the tip.

5.2. Spin-polarized surface states on Co nanoislands

Since the late 1990s it has been known that triangular bilayer Co islands can self-assemble on the (111) surface of Cu under certain environmental parameters (Co coverage, deposition or annealing temperature etc) [191]. Co deposited on Cu(111) forms islands of almost perfect triangular shape due to anisotropic edge diffusion. Islands can grow on both fcc and hcp sites of the supporting Cu(111) surface [185, 191].

Due to their large lateral extent such islands can harbor a surface state similar to that existing on Co monolayers. The spin-polarized nature of these surface states was theoretically predicted in 2003 [183]. It was shown that majority and minority states have principally different dispersion laws around the Fermi energy: while the majority state is a Shockley 2D-free-electron-like surface state, with a band bottom at -0.233 eV, its minority counterpart resides at much higher energies (~ 0.8 eV). The minority valence band around the Fermi energy is dominated by a virtually non-dispersive state with a high negative effective electron mass. These findings perfectly supported available STS results. Later, the spin-polarized nature of surface states on Co nanoislands was demonstrated directly by means of spin-polarized STS experiments [184, 173, 73, 174].

This difference in dispersion laws drew particular attention to the phenomenon of spin-polarized confinement of electrons on Co nanoislands [183, 185, 182, 73]. In a nutshell, while the majority free-like Shockley surface state is confined, forming near and above the Fermi energy a pronounced standing wave pattern [184, 185, 182, 73], minority states are non-dispersive everywhere except a relatively narrow window of energies around 0.25 eV below the Fermi level [183–185, 182, 73]. This can lead to the formation of standing waves of polarization [185]. The sign of polarization is actually determined by the level of minority states. At energies where the minority LDOS dominates, the polarization is negative. Where the majority LDOS has higher amplitude, the polarization is positive. Most interesting is, however, the situation when the densities of majority and minority electrons are close. In this case the polarization can be positive on the crest of the majority standing wave and negative in its trough. Such local modulation of the polarization also leads to local oscillation of the TMR, which can be directly measured in an STM experiment [174]. This is the first option of locally tailoring the TMR highlighted by Ignatiev *et al* [75].

Here we shall be interested in the second possibility discussed in the latter paper—the possibility to tune TMR and spin-polarization related to the band structure manipulation by means of external bias (electric field). The fact that Shockley surface states are sensitive to applied EEF has been recently discussed [171, 172, 74, 155]. Briefly, we have already touched the subject in the introduction (section 1.3.4). The external electric field affects the evanescent tails of the surface state reaching into the vacuum (see figure 1(d)). Fields directed towards the surface create an attractive potential, which weakens the confinement by the vacuum barrier and increases the spill-out of electrons, which screen the EEF. As a result, the surface state bands shifts to lower energies and the surface state LDOS increases in the vacuum. Oppositely

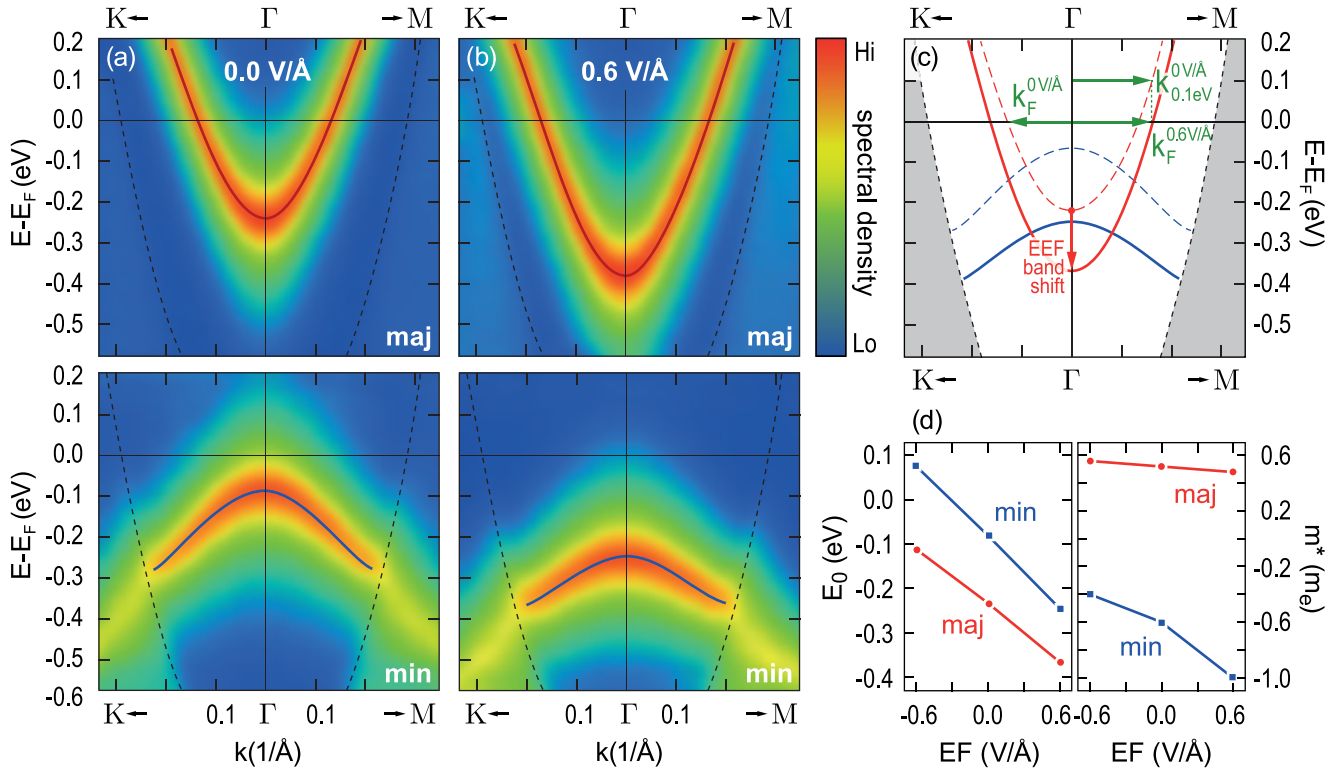


Figure 23. (a), (b) Spectral density maps of majority (top panels) and minority (bottom panels) states along the $K-\bar{\Gamma}-M$ path in the vicinity of the $\bar{\Gamma}$ point plotted for electric fields of (a) 0.0 V/\AA and (b) $+0.6 \text{ V/\AA}$. The boundaries of the projected bandgap of Cu(111) are outlined by dashed contours. The bands are traced by red (majority) and blue (minority) lines. (c) A sketch of the band structure and the field induced shifts. The dashed lines show the zero external field case. The solid lines stand for the band structure in the field of 0.6 V/\AA . Majority and minority bands are plotted with red and blue curves, respectively. The gray shaded area shows the bulk state continuum. (d) The binding energies (E_0) and effective masses (m^*) of majority (red circles) and minority (blue squares) surface bands are plotted. Figure adapted with permission from [75] The American Physical Society, copyright 2012.

directed fields have a contrary effect, i.e. they confine electrons and raise the surface state binding energies. If surface states are spin-polarized, then majority- and minority-spin electrons are affected differently. It thus stands to reason that on changing the band structure with external bias we also change the spin-polarized confinement features discussed above and with them the local TMR ratio.

Now let us see how those two concepts work in practice or, to be quite precise, in theory. The band structures of bilayer Co nanoislands on a Cu(111) surface were studied by Ignatiev *et al* [75] with a well established density functional theory technique—the Korringa–Kohn–Rostoker Green’s function method (KKR–GF), suitable for dealing with electric fields [74]. As a model system, an island two atomic layers high and with a base length of $\sim 12 \text{ nm}$ was used—the same size as was considered experimentally in [73].

The spectral electron-density maps (SDMs)² of majority and minority electrons some 5 \AA above a Co bilayer without an external field are presented in figure 23(a). As expected, the majority Shockley surface state (traced by a red line in the upper panel of figure 23(a)) can be observed inside the projected bulk bandgap of the Cu(111) surface (the outline of

the gap is denoted by dashed lines in figure 23(a)). The surface state binding energy is -0.25 eV . Minority states (traced by a blue line in the lower panel of figure 23(a)) form a lightly dispersive band stemming from the d states in the Co bilayer. This band has a negative effective mass and a binding energy of -0.1 eV . Where it crosses the boundary of the bandgap and overlaps with the Cu(111) bulk states, surface resonances appear (at about -0.4 eV in figure 23(a)).

Both majority and minority surface state bands are shifted in energy upon exposure to the EEF. This phenomenon (the so called screening) is illustrated in figure 23(b). Here the band structure of the same bilayer Co nanoisland exposed to an EEF of $+0.6 \text{ V/\AA}$ is presented. The positive sign corresponds to fields directed towards the surface. Aside from the apparent energy shift of the bands, it can be noted that, while the majority surface state remains virtually unchanged in shape (shifts rigidly), the minority band becomes less dispersive (the effective mass is increased in amplitude). Switching the applied electric field from $+0.6 \text{ V/\AA}$ to -0.6 V/\AA shifts the binding energies of majority and minority states from -0.37 to -0.12 eV and from -0.25 to $+0.07 \text{ eV}$, respectively. In this case both majority and dispersive minority states are non-zero at the Fermi energy. The shifting of the bands under the influence of the EEF is sketched in figure 23(c) and a summary of the band-bottom positions and effective masses is given in figure 23(d).

² The SDM is a plot of the k -vector and energy resolved LDOS at a point in vacuum for a set of k -points along the $K-\bar{\Gamma}-M$ line in the Brillouin zone and for a given energy window.

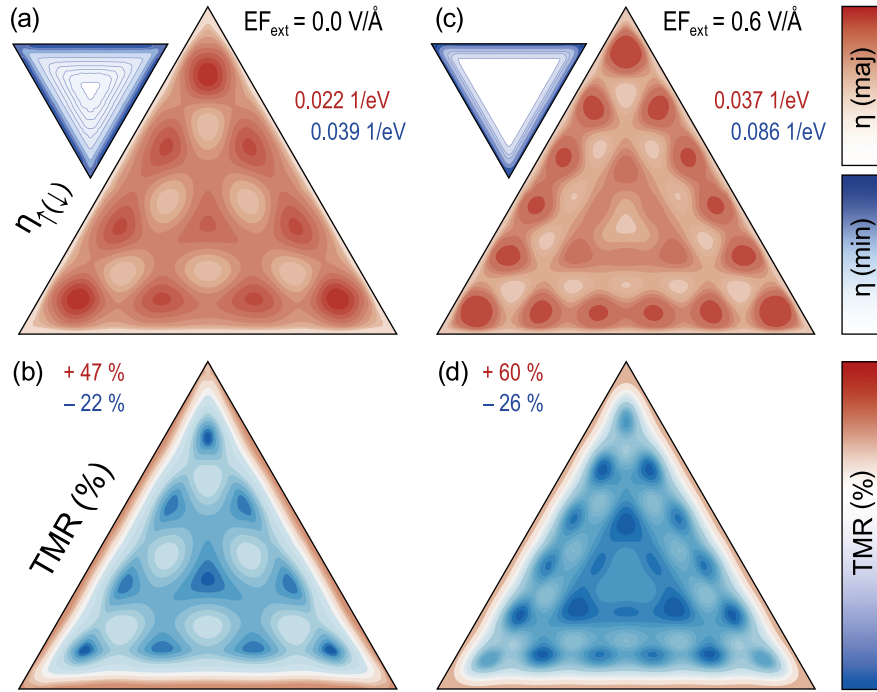


Figure 24. (a), (c) Electron densities of states for E_F for zero EEF (a) and $EF = 0.6 \text{ V/\AA}$ (c) are plotted for majority and minority (insets) electrons. The color map is given on the right of the figure. The numbers next to electron density of states distributions denote (top to bottom) the current strength of the EEF for which the map is plotted and the maximum values of the majority (red) and minority (blue) electron densities. The minimal values are always 0 eV^{-1} (white). (b), (d) The TMR distribution maps for the above cases, calculated with equations (9) and (6). The polarization of the tip has been assumed to be 0.2. The numbers next to the maps denote the boundaries of the color scale. White always corresponds to zero TMR. Figure adapted with permission from [75] The American Physical Society, copyright 2012.

5.3. Standing wave patterns and TMR

Now let us see how the spin-polarized confinement and the external field sensitivity of the surface bands can be used to locally control the polarization of surface electrons and TMR ratio. As discussed above, in the absence of an EEF the majority band of the surface state above a bilayer Co island has a binding energy of -0.233 eV and an effective mass of $0.52 m_e$. This band crosses the Fermi energy at $k_F^{0 \text{ V/\AA}} = 0.127 \text{ 1/\AA}$. The corresponding Fermi wavevector is shown in figure 23(c). The minority band lies below the Fermi energy and has a negative effective mass and hence has no corresponding Fermi wavevector. The minority states, however, still create a background density which contributes to spin-polarization. The confinement of majority electrons at the Fermi energy by the vacuum potential at the boundaries of the island produces a standing wave pattern shown in figure 24(a). The characteristic lateral dimension of the standing wave pattern is in accord with the expected Fermi wavelength of $\lambda_F = \pi/k_F^{0 \text{ V/\AA}} = 24.7 \text{ \AA}$. The minority electrons are not expected to be confined, which is indeed the case (see inset in figure 24(a)). If we now use equation (9) to calculate the local TMR ratio, we obtain the distribution shown in figure 24(b). At the edge of the island the TMR is dictated by the prevailing minority edge states (inset figure 24(a)) and is positive (red color code), while in the center of the island the densities of majority and minority states are comparable and the standing wave patterns in the majority density determine

the polarization and the TMR ratio. The latter varies from almost 0 (white) to -22% (blue).

If an EEF is applied the picture immediately changes. Upon exposure of the nanoisland to an external field of 0.6 V/\AA both majority and minority bands shift downward in energy by 0.133 and 0.164 eV , respectively (figures 23(c) and (d)). For the electrons at the Fermi energy this means that the influence of the minority state is once again reduced and the majority surface state band crosses the Fermi energy at higher k , giving the majority electrons a $k_F^{0.6 \text{ V/\AA}}$ of 0.152 1/\AA (figure 23(c)). The corresponding TMR maps for an island in an external field of 0.6 V/\AA are shown in figure 24(d). The change in majority and minority DOS distributions are directly reflected in the TMR map. Choosing an appropriate point within the island, one can switch the local polarization of surface state electrons on and off by applying EEF and correspondingly tailor the TMR ratio of electrons confined to the bilayer Co nanoisland.

It can be noted that if we apply the opposite electric field or go to lower energies for observations we shall eventually encounter an energy window where the minority states become dispersive (in the confines of the minority (blue) band in figure 23(c)). At these energies either the confinement of minority electrons or both minority and majority confinements will be the determining factor for the local polarization and TMR distributions. In the latter case the TMR map will be composed of two overlapping standing wave patterns of different or similar wavelengths and is likely to be fairly complex.

6. Conclusions

To summarize, among the different flavors of magneto-electric coupling effects, the use of external electric field is one of the favorites when it comes to metallic surfaces and nanostructures. External non-zero bias invokes an electron redistribution at the interface/surface, which inevitably changes local electronic properties. In magnetic systems this screening can have a spin-polarized character, directly affecting the magnetism of the surface/interface, but even in non-magnetic systems the EEF can lead to the emergence of ferromagnetism, e.g. if the materials of the systems are prone to falling victim to the Stoner instability. This effect can be used to tailor single spins at the surface, enhance or reduce the magnetic anisotropy or even change the easy axis of magnetization in layered systems.

The effect of the EEF can be significantly enhanced by the use of an electrolyte or an ionic film. The latter create an excess charge above the surface affecting the magnetism of the system both on the chemical level of direct interactions and by bringing a sizable amount of excess electron or hole charge, which acts similarly to the EEF, yet on a larger scale. It can be applied, e.g. for control of magnetic anisotropies of metallic alloyed multilayers or for tailoring the exchange interaction of single substitutional impurities.

If the system of interest is not coupled to an infinite bath of electrons/holes, such as a metal bulk, it can be charged directly by injecting the corresponding carriers via tunneling and thus directly tailoring their density in the system. The achieved effects are almost identical to those of electrolyte application in kind and magnitude.

Finally, not only localized atomic spins and related parameters can be controlled by EEF and charging, but also the local polarization of quasi-free electrons, such as the Shockley surface state confined to surface nanostructures. Here the effect is based on the Stark-like shift of the bands by EEF, which directly relates to the confinement patterns and, finally, to the local polarization and tunneling magnetoresistance ratios in the system.

Acknowledgments

The authors would like to thank Pavel A Ignatiev, Nikolay N Negulyaev, Lucila Juárez-Reyes, Larissa Niebergall, Kun Tao, Jürgen Kirschner, Wolfram Hergert and Gustavo M Pastor for helpful discussions and support.

The financial support of the Deutsche Forschungsgemeinschaft (SFB 762 and project ‘Structure and magnetism of cluster ensembles on metal surfaces: microscopic theory of the fundamental interactions’) is also gratefully acknowledged.

References

- [1] Wolf S A, Awschalom D D, Buhrman R A, Daughton J M, von Molnár S, Roukes M L, Chtchelkanova A Y and Treger D M 2001 *Science* **294** 1488
- [2] Žutić I and Das Sarma S 2004 *Rev. Mod. Phys.* **76** 323
- [3] Prinz G A 1998 *Science* **282** 1660
- [4] Lenk B, Ulrichs H, Garbs F and Münzenberg M 2011 *Phys. Rep.* **507** 107
- [5] Khitun A, Bao M and Wang K L 2010 *J. Phys. D: Appl. Phys.* **43** 264005
- [6] Schneider T, Serga A A, Leven B, Hillebrands B, Stamps R L and Kostylev M P 2008 *Appl. Phys. Lett.* **92** 022505
- [7] Piramanayagam S N and Chong T C (ed) 2011 *Developments in Data Storage* (Hoboken, NJ: Wiley)
- [8] Rottmayer R *et al* 2006 *IEEE Trans. Magn.* **42** 2417
- [9] Slonczewski J 1996 *J. Magn. Magn. Mater.* **159** L1
- [10] Berger L 1996 *Phys. Rev. B* **54** 9353
- [11] Katine J and Fullerton E E 2008 *J. Magn. Magn. Mater.* **320** 1217
- [12] Loth S, Baumann S, Lutz C P, Eigler D M and Heinrich A J 2012 *Science* **335** 196
- [13] Spaldin N A and Fiebig M 2005 *Science* **309** 391
- [14] Fiebig M 2005 *J. Phys. D: Appl. Phys.* **38** R123
- [15] Kimura T, Goto T, Shintani H, Ishizaka K, Arima T and Tokura Y 2003 *Nature* **426** 55
- [16] Lonkai T, Tomuta D, Amann U, Ihringer J, Hendriks R, Többsen D and Mydosh J 2004 *Phys. Rev. B* **69** 134108
- [17] Lottermoser T, Lonkai T, Amann U, Hohlwein D, Ihringer J and Fiebig M 2004 *Nature* **430** 541
- [18] Tokura Y 2006 *Science* **312** 1481
- [19] Eerenstein W, Mathur N D and Scott J F 2006 *Nature* **442** 759
- [20] Sahoo S, Polisetty S, Duan C-G, Jaswal S, Tsymbal E and Binek C 2007 *Phys. Rev. B* **76** 092108
- [21] Chu Y-H *et al* 2008 *Nature Mater.* **7** 478
- [22] Saito M, Ishikawa K, Konno S, Taniguchi K and Arima T 2009 *Nature Mater.* **8** 634
- [23] Choi Y J, Zhang C L, Lee N and Cheong S-W 2010 *Phys. Rev. Lett.* **105** 097201
- [24] Ding H-C and Duan C-G 2012 *Europhys. Lett.* **97** 57007
- [25] Babkevich P, Poole A, Johnson R D, Roessli B, Prabhakaran D and Boothroyd A T 2012 *Phys. Rev. B* **85** 134428
- [26] Babkevich P, Poole A, Johnson R D, Roessli B, Prabhakaran D and Boothroyd A T 2012 *Phys. Rev. B* **86** 019905
- [27] Hearmon A J, Fabrizi F, Chapon L C, Johnson R D, Prabhakaran D, Streltsov S V, Brown P J and Radaelli P G 2012 *Phys. Rev. Lett.* **108** 237201
- [28] Chen Y, Fitchorov T, Cai Z, Ziemer K S, Vittoria C and Harris V G 2010 *J. Phys. D: Appl. Phys.* **43** 155001
- [29] Brivio S, Petti D, Bertacco R and Cezar J C 2011 *Appl. Phys. Lett.* **98** 092505
- [30] Rovillain P, de Sousa R, Gallais Y, Sacuto A, Méasson M A, Colson D, Forget A, Bibes M, Barthélémy A and Cazayous M 2010 *Nature Mater.* **9** 975
- [31] Lebeugle D, Mougou A, Viret M, Colson D and Ranno L 2009 *Phys. Rev. Lett.* **103** 257601
- [32] Chiba D, Sawicki M, Nishitani Y, Nakatani Y, Matsukura F and Ohno H 2008 *Nature* **455** 515
- [33] Yamada Y, Ueno K, Fukumura T, Yuan H T, Shimotani H, Iwasa Y, Gu L, Tsukimoto S, Ikuhara Y and Kawasaki M 2011 *Science* **332** 1065
- [34] Güçlü A D, Potasz P and Hawrylak P 2011 *Phys. Rev. B* **84** 035425
- [35] Lu Y-H, Shi L, Zhang C and Feng Y-P 2009 *Phys. Rev. B* **80** 233410
- [36] Michetti P, Recher P and Iannaccone G 2010 *Nano Lett.* **10** 4463
- [37] Otani M, Takagi Y, Koshino M and Okada S 2010 *Appl. Phys. Lett.* **96** 242504
- [38] Gütllich P, Hauser A and Spiering H 1994 *Angew. Chem. Int. Edn* **106** 2109

- [39] Real J A, Gaspar A B, Niel V and Muñoz M 2003 *Coord. Chem. Rev.* **236** 121
- [40] Gaspar A B, Ksenofontov V, Seredyuk M and Gütllich P 2005 *Coord. Chem. Rev.* **249** 2661
- [41] Sato O, Iyoda T, Fujishima A and Hashimoto K 1996 *Science* **272** 704
- [42] Sato O, Tao J and Zhang Y-Z 2007 *Angew. Chem. Int. Edn* **46** 2152
- [43] Sato O, Tao J and Zhang Y-Z 2007 *Angew. Chem. Int. Edn* **119** 2200
- [44] Sato O, Einaga Y, Fujishima A and Hashimoto K 1999 *Inorg. Chem.* **38** 4405
- [45] Zyazin A S *et al* 2010 *Nano Lett.* **10** 3307
- [46] Bosch-Serrano C, Clemente-Juan J M, Coronado E, Gaita-Ariño A, Palií A and Tsukerblat B 2012 *ChemPhysChem* **13** 2662
- [47] Xiu F, Wang Y, Zou J and Wang K L 2011 *Nano Rev.* **2** 1
- [48] Boukari H, Kossacki P, Bertolini M, Ferrand D, Cibert J, Tatarenko S, Wasieła A, Gaj J and Dietl T 2002 *Phys. Rev. Lett.* **88** 207204
- [49] De A, Pryor C and Flatté M 2009 *Phys. Rev. Lett.* **102** 017603
- [50] Nepal N, Luen M O, Zavada J M, Bedair S M, Frajtag P and El-Masry N A 2009 *Appl. Phys. Lett.* **94** 132505
- [51] Ohno H, Chiba D, Matsukura F, Omiya T, Abe E, Dietl T, Ohno Y and Ohtani K 2000 *Nature* **408** 944
- [52] Xuan H C, Wang L Y, Zheng Y X, Li Y L, Cao Q Q, Chen S Y, Wang D H, Huang Z G and Du Y W 2011 *Appl. Phys. Lett.* **99** 032509
- [53] Das J, Li M, Kalarickal S S, Altmannshofer S, Buchanan K S, Li J F and Viehland D 2010 *Appl. Phys. Lett.* **96** 222508
- [54] Ding H, Cheah J W, Chen L, Sritharan T and Wang J 2012 *Thin Solid Films* **522** 420
- [55] Khalili Amiri P, Upadhyaya P, Alzate J G and Wang K L 2013 *J. Appl. Phys.* **113** 013912
- [56] Kita K, Abraham D W, Gajek M J and Worledge D C 2012 *J. Appl. Phys.* **112** 033919
- [57] Kum H, Basu D, Bhattacharya P and Guo W 2009 *Appl. Phys. Lett.* **95** 212503
- [58] Murakawa H, Onose Y and Tokura Y 2009 *Phys. Rev. Lett.* **103** 147201
- [59] Niazi T, Cormier M, Lucot D, Largeau L, Jeudy V, Cibert J and Lemaître A 2013 *Appl. Phys. Lett.* **102** 122403
- [60] Ryan P J *et al* 2013 *Nature Commun.* **4** 1334
- [61] Wang W-G, Li M, Hageman S and Chien C L 2012 *Nature Mater.* **11** 64
- [62] Zhang S 1999 *Phys. Rev. Lett.* **83** 640
- [63] Dasa T R, Ignatiev P A and Stepanyuk V S 2012 *Phys. Rev. B* **85** 205447
- [64] Negulyaev N N, Stepanyuk V S, Hergert W and Kirschner J 2011 *Phys. Rev. Lett.* **106** 037202
- [65] Baldelli S 2008 *Acc. Chem. Res.* **41** 421
- [66] Weisheit M, Fähler S, Marty A, Souche Y, Poinsignon C and Givord D 2007 *Science* **315** 349
- [67] Juárez-Reyes L, Pastor G M and Stepanyuk V S 2012 *Phys. Rev. B* **86** 235436
- [68] Ruiz-Díaz P, Dasa T R and Stepanyuk V S 2013 *Phys. Rev. Lett.* **110** 267203
- [69] Gartland P O and Slagsvold B J 1975 *Phys. Rev. B* **12** 4047
- [70] Reinert F, Nicolay G, Schmidt S, Ehm D and Hüfner S 2001 *Phys. Rev. B* **63** 115415
- [71] Goldmann A, Dose V and Borstel G 1985 *Phys. Rev. B* **32** 1971
- [72] Kevan S 1983 *Phys. Rev. Lett.* **50** 526
- [73] Oka H, Ignatiev P A, Wedekind S, Rodary G, Niebergall L, Stepanyuk V S, Sander D and Kirschner J 2010 *Science* **327** 843
- [74] Ignatiev P A and Stepanyuk V S 2011 *Phys. Rev. B* **84** 075421
- [75] Ignatiev P A, Brovko O O and Stepanyuk V S 2012 *Phys. Rev. B* **86** 045409
- [76] Hirjibehedin C F, Lutz C P and Heinrich A J 2006 *Science* **312** 1021
- [77] Thomas L, Lioni F, Ballou R, Gatteschi D, Sessoli R and Barbara B 1996 *Nature* **383** 145
- [78] Sessoli R, Gatteschi D, Caneschi A and Novak M A 1993 *Nature* **365** 141
- [79] Friedman J R, Sarachik M P, Tejada J and Ziolo R 1996 *Phys. Rev. Lett.* **76** 3830
- [80] Pederson M and Khanna S 1999 *Phys. Rev. B* **59** R693
- [81] Boukhvalov D, Lichtenstein A, Dobrovitski V, Katsnelson M, Harmon B, Mazurenko V and Anisimov V 2002 *Phys. Rev. B* **65** 184435
- [82] Barraza-Lopez S, Avery M and Park K 2007 *Phys. Rev. B* **76** 224413
- [83] Stepanyuk V, Hergert W, Wildberger K, Nayak S and Jena P 1997 *Surf. Sci.* **384** L892
- [84] Stepanyuk V, Hergert W, Rennert P, Wildberger K, Zeller R and Dederichs P 1997 *Solid State Commun.* **101** 559
- [85] Kahn O 1998 *Science* **279** 44
- [86] He Y, Wei X, Chan C and Che J 2005 *Phys. Rev. B* **71** 045401
- [87] Kellogg G 1993 *Phys. Rev. Lett.* **70** 1631
- [88] Feibelman P 2001 *Phys. Rev. B* **64** 125403
- [89] Jiang N, Zhang Y Y, Liu Q, Cheng Z H, Deng Z T, Du S X, Gao H-J, Beck M J and Pantelides S T 2010 *Nano Lett.* **10** 1184
- [90] Yoon B and Landman U 2008 *Phys. Rev. Lett.* **100** 056102
- [91] Zhou J, Wang Q, Sun Q, Jena P and Chen X S 2010 *Proc. Natl. Acad. Sci. USA* **107** 2801
- [92] Zhou J, Wang Q, Sun Q, Jena P and Chen X S 2009 arXiv:0903.3079 [cond-mat]
- [93] Troparevsky M C, Zhao K, Xiao D, Zhang Z and Eguluz A G 2009 *Nano Lett.* **9** 4452
- [94] Duan C-G, Jaswal S and Tsymbal E 2006 *Phys. Rev. Lett.* **97** 047201
- [95] Baadji N, Piacenza M, Tugsuz T, Della Sala F, Maruccio G and Sanvito S 2009 *Nature Mater.* **8** 813
- [96] Gamble S, Burkhardt M, Kashuba A, Allenspach R, Parkin S, Siegmann H and Stöhr J 2009 *Phys. Rev. Lett.* **102** 217201
- [97] Sun Y, Burton J D and Tsymbal E Y 2010 *Phys. Rev. B* **81** 064413
- [98] Stoner E C 1936 *Proc. R. Soc. Lond. A* **154** 656
- [99] Duan C-G, Velez J, Sabirianov R, Zhu Z, Chu J, Jaswal S and Tsymbal E 2008 *Phys. Rev. Lett.* **101** 137201
- [100] Nakamura K, Shimabukuro R, Fujiwara Y, Akiyama T, Ito T and Freeman A 2009 *Phys. Rev. Lett.* **102** 187201
- [101] Zhang H, Richter M, Koepfner K, Opahle I, Tasnádi F and Eschrig H 2009 *New J. Phys.* **11** 043007
- [102] Chiba D, Nakatani Y, Matsukura F and Ohno H 2010 *Appl. Phys. Lett.* **96** 192506
- [103] Alexander S and Anderson P W 1964 *Phys. Rev.* **133** A1594
- [104] Nayak S K, Rao B K and Jena P 1998 *J. Phys.: Condens. Matter* **10** 10863
- [105] Gambardella P *et al* 2003 *Science* **300** 1130
- [106] Błoński P and Hafner J 2009 *J. Phys.: Condens. Matter* **21** 426001
- [107] Baud S, Ramseyer C, Bihlmayer G and Blügel S 2006 *Phys. Rev. B* **73** 104427

- [108] Gambardella P, Dallmeyer A, Maiti K, Malagoli M C, Eberhardt W, Kern K and Carbone C 2002 *Nature* **416** 301
- [109] Lazarovits B, Szunyogh L and Weinberger P 2003 *Phys. Rev. B* **67** 024415
- [110] Rusponi S, Cren T, Weiss N, Epple M, Bulushek P, Claude L and Brune H 2003 *Nature Mater.* **2** 546
- [111] Balashov T *et al* 2009 *Phys. Rev. Lett.* **102** 257203
- [112] Błoński P, Lehnert A, Dennler S, Rusponi S, Eitzkorn M, Moulas G, Bencok P, Gambardella P, Brune H and Hafner J 2010 *Phys. Rev. B* **81** 104426
- [113] Röder H, Hahn E, Brune H, Bucher J-P and Kern K 1993 *Nature* **366** 141
- [114] Stekolnikov A, Bechstedt F, Wisniewski M, Schäfer J and Claessen R 2008 *Phys. Rev. Lett.* **100** 196101
- [115] Wei D H, Gao C L and Zakeri K 2009 *Phys. Rev. Lett.* **103** 225504
- [116] Nilius N, Wallis T M and Ho W 2002 *Science* **297** 1853
- [117] Braun K-F and Rieder K-H 2002 *Phys. Rev. Lett.* **88** 096801
- [118] Fölsch S, Hyldgaard P, Koch R and Ploog K 2004 *Phys. Rev. Lett.* **92** 056803
- [119] Lagoute J J, Nacci C and Fölsch S 2007 *Phys. Rev. Lett.* **98** 146804
- [120] Negulyaev N N, Stepanyuk V S, Niebergall L, Bruno P, Hergert W, Repp J, Rieder K-H and Meyer G 2008 *Phys. Rev. Lett.* **101** 226601
- [121] Khajetoorians A A, Wiebe J, Chilian B and Wiesendanger R 2011 *Science* **332** 1062
- [122] Tsymbal E Y 2012 *Nature Mater.* **11** 12
- [123] Tsujikawa M and Oda T 2009 *Phys. Rev. Lett.* **102** 247203
- [124] Hu J and Wu R 2013 *Phys. Rev. Lett.* **110** 097202
- [125] Neugebauer J and Scheffler M 1992 *Phys. Rev. B* **46** 16067
- [126] Gambardella P, Dallmeyer A, Maiti K, Malagoli M, Rusponi S, Ohresser P, Eberhardt W, Carbone C and Kern K 2004 *Phys. Rev. Lett.* **93** 077203
- [127] Ortega J and Himpfel F 1992 *Phys. Rev. Lett.* **69** 844
- [128] Freeman A and Wu R-Q 1991 *J. Magn. Magn. Mater.* **100** 497
- [129] Weber W, Bischof A, Allenspach R, Würsch C, Back C and Pescia D 1996 *Phys. Rev. Lett.* **76** 3424
- [130] Altmann K, O'Brien W, Seo D, Himpfel F, Ortega J, Naermann A, Segovia P, Mascaraque A and Michel E 1999 *J. Electron Spectrosc. Relat. Phenom.* **101–103** 367
- [131] Lu Z-Y, Zhang X-G and Pantelides S 2005 *Phys. Rev. Lett.* **94** 207210
- [132] Yoshimatsu K, Horiba K, Kumigashira H, Yoshida T, Fujimori A and Oshima M 2011 *Science* **333** 319
- [133] Luh D, Paggel J, Miller T and Chiang T 2000 *Phys. Rev. Lett.* **84** 3410
- [134] Park J S *et al* 2011 *Phys. Rev. B* **83** 113405
- [135] Li J, Przybylski M, Yildiz F, Ma X and Wu Y 2009 *Phys. Rev. Lett.* **102** 207206
- [136] Bauer U, Dabrowski M, Przybylski M and Kirschner J 2011 *Phys. Rev. B* **84** 144433
- [137] Nakamura K, Shimabukuro R, Akiyama T, Ito T and Freeman A 2009 *Phys. Rev. B* **80** 172402
- [138] Maruyama T *et al* 2009 *Nature Nanotechnol.* **4** 158
- [139] Subkow S and Fähnle M 2011 *Phys. Rev. B* **84** 220409
- [140] Shimamura K, Chiba D, Ono S, Fukami S, Ishiwata N, Kawaguchi M, Kobayashi K and Ono T 2012 *Appl. Phys. Lett.* **100** 122402
- [141] Dasa T R, Ruiz-Díaz P, Brovko O O and Stepanyuk V S 2013 *Phys. Rev. B* **88** 104409
- [142] Simon E, Újfalussy B, Lazarovits B, Szilva A, Szunyogh L and Stocks G M 2011 *Phys. Rev. B* **83** 224416
- [143] Patrone P N and Einstein T L 2012 *Phys. Rev. B* **85** 045429
- [144] Simon E, Újfalussy B, Szilva A and Szunyogh L 2010 *J. Phys.: Conf. Ser.* **200** 032067
- [145] Stepanyuk V, Baranov A, Tsvilín D, Hergert W, Bruno P, Knorr N, Schneider M and Kern K 2003 *Phys. Rev. B* **68** 205410
- [146] Brovko O O, Stepanyuk V S and Bruno P 2008 *Phys. Rev. B* **78** 165413
- [147] Brovko O O, Ignatiev P A, Stepanyuk V S and Bruno P 2008 *Phys. Rev. Lett.* **101** 36809
- [148] Brovko O O and Stepanyuk V S 2010 *Phys. Status Solidi* **247** 1161
- [149] Néel N, Berndt R, Kröger J, Wehling T O, Lichtenstein A I and Katsnelson M I 2011 *Phys. Rev. Lett.* **107** 106804
- [150] Zhou L, Wiebe J, Lounis S, Vedmedenko E, Meier F, Blügel S, Dederichs P H and Wiesendanger R 2010 *Nature Phys.* **6** 187
- [151] Meier F, Zhou L, Wiebe J and Wiesendanger R 2008 *Science* **320** 82
- [152] Wahl P, Simon P, Diekhöner L, Stepanyuk V, Bruno P, Schneider M and Kern K 2007 *Phys. Rev. Lett.* **98** 056601
- [153] Stepanyuk V, Niebergall L, Longo R, Hergert W and Bruno P 2004 *Phys. Rev. B* **70** 75414
- [154] Zhang X P, Miao B F, Sun L, Gao C L, Hu A, Ding H F and Kirschner J 2010 *Phys. Rev. B* **81** 125438
- [155] Berland K, Einstein T L and Hyldgaard P 2012 *Phys. Rev. B* **85** 035427
- [156] Schnur S and Groß A 2011 *Catal. Today* **165** 129
- [157] Hyldgaard P and Persson M 2000 *J. Phys.: Condens. Matter* **12** L13
- [158] Drittler B, Weinert M, Zeller R and Dederichs P 1989 *Phys. Rev. B* **39** 930
- [159] Gong S J, Duan C-G, Zhu Z-Q and Chu J-H 2012 *Appl. Phys. Lett.* **100** 122410
- [160] Si C, Duan W, Liu Z and Liu F 2012 *Phys. Rev. Lett.* **109** 226802
- [161] Schull G, Dappe Y J, González C, Bulou H and Berndt R 2011 *Nano Lett.* **11** 3142
- [162] Bazhиров T and Cohen M L 2013 *J. Phys.: Condens. Matter* **25** 105506
- [163] Aihara S, Kageshima H, Sakai T and Sato T 2012 *J. Appl. Phys.* **112** 073910
- [164] Repp J, Meyer G, Olsson F E and Persson M 2004 *Science* **305** 493
- [165] Shen Y, Guo S, Hu J and Zhang Y 2012 *Appl. Phys. Lett.* **101** 183109
- [166] Zdrojek M, Mèlin T, Boyaval C, Stiévenard D, Jouault B, Wozniak M, Huczko A, Gebicki W and Adamowicz L 2005 *Appl. Phys. Lett.* **86** 213114
- [167] Haraguchi S, Tsujikawa M, Gotou J and Oda T 2011 *J. Phys. D: Appl. Phys.* **44** 064005
- [168] Wang D-S, Wu R and Freeman A 1993 *Phys. Rev. B* **47** 14932
- [169] Bruno P 1989 *Phys. Rev. B* **39** 865
- [170] Andersson C, Sanyal B, Eriksson O, Nordström L, Karis O, Arvanitis D, Konishi T, Holub-Krappe E and Dunn J 2007 *Phys. Rev. Lett.* **99** 177207
- [171] Limot L, Maroutian T, Johansson P and Berndt R 2003 *Phys. Rev. Lett.* **91** 196801
- [172] Kröger J, Limot L, Jensen H, Berndt R and Johansson P 2004 *Phys. Rev. B* **70** 033401
- [173] Pietzsch O, Okatov S, Kubetzka A, Bode M, Heinze S, Lichtenstein A and Wiesendanger R 2006 *Phys. Rev. Lett.* **96** 237203
- [174] Oka H, Tao K, Wedekind S, Rodary G, Stepanyuk V S, Sander D and Kirschner J 2011 *Phys. Rev. Lett.* **107** 187201

- [175] Alferov Z I 1998 *Semiconductors* **32** 1
- [176] Julliere M 1975 *Phys. Lett. A* **54** 225
- [177] De Teresa J M 1999 *Science* **286** 507
- [178] Tsymbal E Y, Mryasov O N and LeClair P R 2003 *J. Phys.: Condens. Matter* **15** R109
- [179] Parkin S S P, Kaiser C, Panchula A, Rice P M, Hughes B, Samant M and Yang S-H 2004 *Nature Mater.* **3** 862
- [180] Heinze S, Nie X, Blügel S and Weinert M 1999 *Chem. Phys. Lett.* **315** 167
- [181] Niranjana M K, Duan C-G, Jaswal S S and Tsymbal E Y 2010 *Appl. Phys. Lett.* **96** 222504
- [182] Niebergall L, Stepanyuk V S, Berakdar J and Bruno P 2006 *Phys. Rev. Lett.* **96** 127204
- [183] Diekhöner L, Schneider M A, Baranov A N, Stepanyuk V S, Bruno P and Kern K 2003 *Phys. Rev. Lett.* **90** 236801
- [184] Rastei M, Heinrich B, Limot L, Ignatiev P, Stepanyuk V, Bruno P and Bucher J 2007 *Phys. Rev. Lett.* **99** 246102
- [185] Pietzsch O, Kubetzka A, Bode M and Wiesendanger R 2004 *Phys. Rev. Lett.* **92** 057202
- [186] Tersoff J and Hamann D R 1983 *Phys. Rev. Lett.* **50** 1998
- [187] Tersoff J and Hamann D R 1985 *Phys. Rev. B* **31** 805
- [188] Slonczewski J 1989 *Phys. Rev. B* **39** 6995
- [189] Wortmann D, Heinze S, Kurz P, Bihlmayer G and Blügel S 2001 *Phys. Rev. Lett.* **86** 4132
- [190] Wiesendanger R 2009 *Rev. Mod. Phys.* **81** 1495
- [191] Negulyaev N, Stepanyuk V, Bruno P, Diekhöner L, Wahl P and Kern K 2008 *Phys. Rev. B* **77** 125437